N71-13098

78	G3
(ACCESSION NUMBER)	(THRU)
(PAGES)	(CODE)
CR-102939	32
(NASA CR OR TMX OR AD NUMBER)	(CATEGORY)

FACILITY FORM 602

Lockheed

HUNTSVILLE RESEARCH & ENGINEERING CENTER

LOCKHEED MISSILES & SPACE COMPANY

A GROUP DIVISION OF LOCKHEED AIRCRAFT CORPORATION

HUNTSVILLE, ALABAMA

32

HREC-1435-1
LMSC/HREC D149171-I

LOCKHEED MISSILES & SPACE COMPANY
HUNTSVILLE RESEARCH & ENGINEERING CENTER
HUNTSVILLE RESEARCH PARK
4800 BRADFORD DRIVE, HUNTSVILLE, ALABAMA

NONLINEAR DYNAMIC ANALYSIS OF STRUCTURES

Final Report

Volume I

NONLINEAR DAMPING IN STRUCTURES

June 1970

Contract NAS8-21435

Prepared for National Aeronautics and Space Administration
Marshall Space Flight Center, Alabama 35812

by

C. S. Chang

APPROVED:

D. McDonald, Manager
Structures & Mechanics Dept.

for J. S. Farrior
Resident Director

FOREWORD

This report presents results of work performed by Lockheed's Huntsville Research & Engineering Center for the Aero-Astronautics Laboratory of NASA-Marshall Space Flight Center under Contract NAS8-21435, "Nonlinear Dynamic Analysis of Structures." This work represents the Phase II effort entitled "Nonlinear Damping in Structures." Printed under separate cover is the Phase II effort, "Structural Joint Damping," LMSC/HREC D149171-II, dated July 1970.

The NASA-MSFC technical monitor for this contract is Mr. Larry A. Kiefling, S&E-AERO-DDS.

SUMMARY

An analytical and experimental study of the dynamic responses of a structure with nonlinear and nonproportional damping is presented.

The analysis showed that the steady-state solution of a structure with damping at its boundary can be obtained from the undamped vibration solutions, and that if nonproportional damping is low, classical normal mode responses are indicated by the derived general solution. The analytical results are used to develop experimental approaches to determine damping properties of substructures or structural elements.

Experimental studies are used to demonstrate the validity of developed techniques.

CONTENTS

Section 1
INTRODUCTION

To predict quantitatively the dynamic responses of a structure, its damping properties must be known accurately. A uniform set of definitions for structural damping properties is not available, however, despite the universally recognized importance. By arbitrarily casting the responses of a structure in the framework of response characteristics of a single-degree-of-freedom oscillator, the term "modal damping coefficient" has been used in many instances to describe the damping of complicated structures. Such an approach, in fact, assumes the response characteristics of the structure from the onset, with modal damping coefficients merely providing values for the already assumed form of the solutions.

Since there is usually no attempt to relate the assumption of modal damping coefficients to physical properties of a structure, it is hardly justifiable to use this type of assumed solution parameters to predict structural responses beyond the experimentally established domain of validity. The usefulness of analyses of this sort is, therefore, rather limited.

Without suitable justification (and sources of supply) of modal damping coefficients, analysis of dynamic responses of complicated structures must use lumped and distributed damping data for structural joints and structural elements (or substructures), respectively. In other words, damping should be considered in the equation of motion before any effort to orthogonalize it is attempted.

For complicated structures, it is impractical to determine local damping properties from dynamic tests of the assembled structure, primarily because many actual dissipative processes in structures are nonlinear in nature and because the distribution of damping mechanisms is usually not proportional to any linear combination of inertia and stiffness matrices. Consequently, the responses of such structures are not solutions of uncoupled modal equations of motion, and local damping properties must be determined by physical substructuring and testing. In general, a substructure or structural element can be so chosen for damping and stiffness measurements that it contains only one relatively simple, continuous member with one or more boundary conditions representing mechanical joints used to connect the substructure with others in the parent structure. For the substructure, damping is due to dissipations which occur within material elements, across joint interfaces (including boundary joints) and over solid-fluid interfaces. In most cases, damping for the substructure is still nonviscous, amplitude-dependent and nonproportional. Because of the simplicity of the substructure, however, the analyses required for damping property measuring experiments can be developed, even with such complications. This is the principal advantage of testing substructures rather than complete structures.

To predict dynamic responses of the parent structure, it may be pointed out that modeling (analytical representation) of structural elements presents relatively minor difficulties, especially in light of recent developments in applications of final element methods. The success or failure of an analysis is critically dependent upon the success or failure in modeling structural joints; and, in particular, in assigning correct stiffness and damping values for joints. Substructure and joint testing will provide the desired information which cannot be easily obtained by any other means. Indeed, a strong case can be easily presented for preferring analyses (or model testing) in combination with substructure tests, over performing full-scale tests on the basis of better accuracy and more meaningful results attainable, usually at lower costs.

The analyses and experiments described in this report provide a detailed demonstration of the technique for handling nonlinear properties (including damping) of a simple structure, which may be considered as a typical substructure of a complicated structure. The booster stage of a structural dynamic model of the Saturn I launch vehicle vas used in the study. The center LOX tank of this booster stage is a typical example of a simple substructure with complicated interface provisions. The study for this structure is developed along the following lines:

1. Solutions are derived for the dynamic responses of a nonuniform beam with a linear, dissipative end condition. (Material and air damping are not included.)

2. Based on results of the analysis, arguments are presented for extending the definition of modal responses of the structure for the case of "low nonproportional damping" contributed by any combination of joint damping, material internal dissipations and air damping.

3. Because it is extremely difficult to introduce nonlinearities exactly into the partial differential equations governing the beam vibrations, and to obtain solutions of the problem, a nonlinear modal equation is postulated. (This equation is constructed on the basis of the solution of the steady-state for the linear problem, and hence, can be regarded only as a format according to which experimentally determined quantities are converted into properties.) For the steady-state, fundamental frequency response solutions are obtained from this nonlinear modal equation. Based on these solutions, experimental approaches are formulated.

4. A set of experiments with the model was performed, and results were used to verify the validity of modal response description. The test and data analyses procedures serve also to demonstrate the practicality of the approach.

While the analyses and experiments of this study are confined to a beam-like structure, they should be easily adaptable to other configurations commonly encountered in aerospace structures.

Section 2
ANALYSES

Responses of a simple substructure with nonlinear, nonproportional damping are considered in this section.

Both nonlinearity and nonproportionality are retained in the analysis because the fundamental application is for developing experimental approaches to measure damping properties, which may well be nonlinear and nonproportional. Only by keeping the analysis general, can the results be used to develop experimental techniques which do not introduce distortion in characterizing the actual properties of the structure. By retaining the true characteristics of damping properties, reasonable extrapolation and extension of data beyond conditions under which they are obtained can be expected.

2.1 VIBRATION OF A BEAM WITH A LINEAR DISSIPATIVE END CONDITION

In accordance with the program outlined in Section 1, an analysis of a non-uniform elastic beam with a dissipative boundary condition is derived. The boundary condition may be linear, first-order viscoelastic or hysteretic in nature. Solutions are derived in terms of undamped modes (but in an unconventional form) of the beam without additional approximations and assumptions. Hence, they are exact to the same degree as the beam theory and the constitutive equations themselves. By introducing additional simplifying approximations, however, conventional model representations can be obtained from the general solutions. Extensions of the method to the analysis of rods and plates, and to include more than one dissipative boundary condition are expected to follow the same line of development. Linear material damping (viscoelastic and/or hysteretic) can be included without difficulty in an approximate manner.

Let w(x, t) be the steady-state forced lateral vibration of the beam in Fig. 1 below. The end $x = \ell$ is free, the end $x = 0$ is a representation of a clamped end. In reality the clamping and the base are not rigid, and are

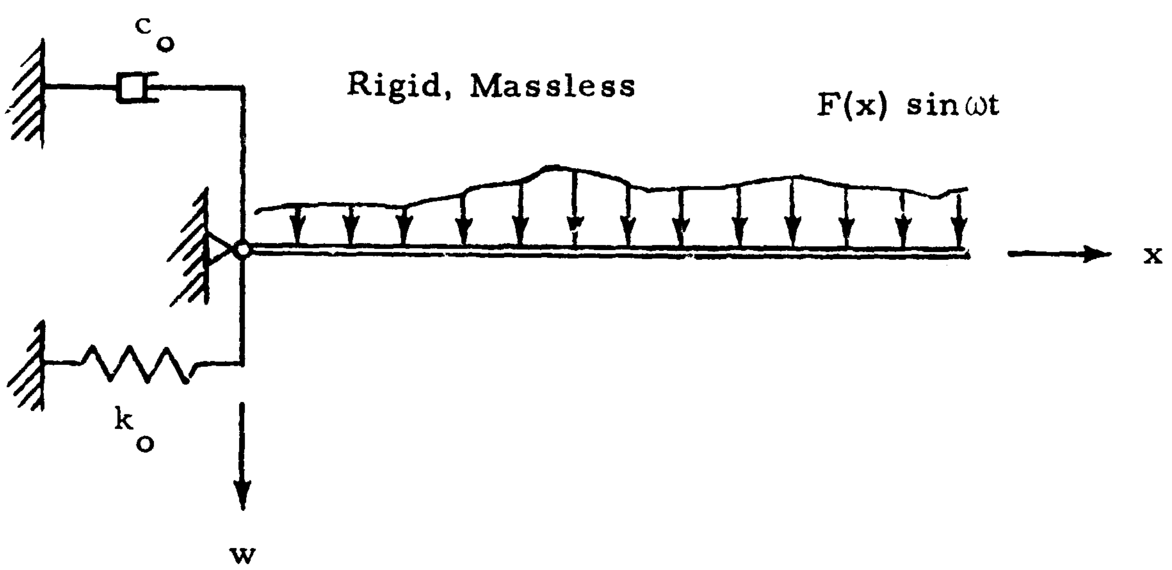

Fig. 1 - Modeling of a Clamped Beam

represented by the pin and the rotational spring. Support damping at $x = 0$ is represented pictorially by the symbol commonly used for linear viscous dashpots, although hysteretic damping can also be treated.

The equations of motion and boundary conditions are

$$\frac{\partial^2}{\partial x^2}\left[EI(x)\,\frac{\partial^2}{\partial x^2}\,w(x,t)\right] + \rho\,\frac{\partial^2}{\partial t^2}\,w(x,t) = F(x)\,\sin\omega t \qquad (1)$$

$$w(o, t) = 0 \tag{2}$$

$$\frac{\partial^2}{\partial x^2} w(\ell, t) = 0 \tag{3}$$

$$\frac{\partial^3}{\partial x^3} w(\ell, t) = 0 \tag{4}$$

and

$$EI(o) \frac{\partial^2}{\partial x^2} w(o, t) = k_o \frac{\partial}{\partial x} w(o, t) + c_o \frac{\partial}{\partial t} \frac{\partial}{\partial x} w(o, t) \tag{5}$$

for a linear viscous dashpot, and

$$EI(o) \frac{\partial^2}{\partial x^2} w(o, t) = k_o \frac{\partial}{\partial x} w(o, t) + g\, H \left[\frac{\partial}{\partial x} w(o, t) \right] \tag{6}$$

for a linear hysteretic damper. All symbols are defined in the Nomenclature at the beginning of this report. The symbol $H[\ \ ]$ denotes the linear hysteresis operator (Ref. 1) and is defined by

$$H\left[A(t)\right] = \int_0^T \phi(\tau)\, A(t - \tau)\, d\tau \tag{7}$$

where T and ϕ are both properties of the damper.

Seek a solution of the form

$$w(x, t) = u(x) \sin\omega t + v(x) \cos\omega t \tag{8}$$

Equations (1) through (5) may be written in terms u(x) and v(x):

$$\left|EI\, u''(x)\right|'' - \rho\omega^2 u(x) = F(x) \tag{9}$$

$$\left|EI\, v''(x)\right|'' - \rho\omega^2 v(x) = 0 \tag{10}$$

$$u_o = u''_\ell = u'''_\ell = 0 \tag{11}$$

$$v_o = v''_\ell = v'''_\ell = 0 \tag{12}$$

$$EI_o\, u''_o - k_o\, u'_o + \omega c_o\, v'_o = 0 \tag{13}$$

$$EI_o\, v''_o - k_o\, v'_o - \omega c_o\, u'_o = 0 \tag{14}$$

where

$$u_o = u(o) \quad , \quad u_\ell = u(\ell)$$

$$v_o = v(o), \ldots, \text{etc.}$$

The following method of analysis is applicable to finding the exact solution of the problem for frequency bands near each resonance. The upper limit of each band is the rigid cantilever frequency and the lower limit, the hinged-free frequency. Since the rotational base stiffness of a clamped beam is non-zero and finite, the resonant frequencies will fall within these bands. The method, therefore, covers all frequency ranges of interest. Figure 2 indicates these frequency bands.

Let

$$\beta = \beta(\omega) = u''_o / v''_o \tag{15}$$

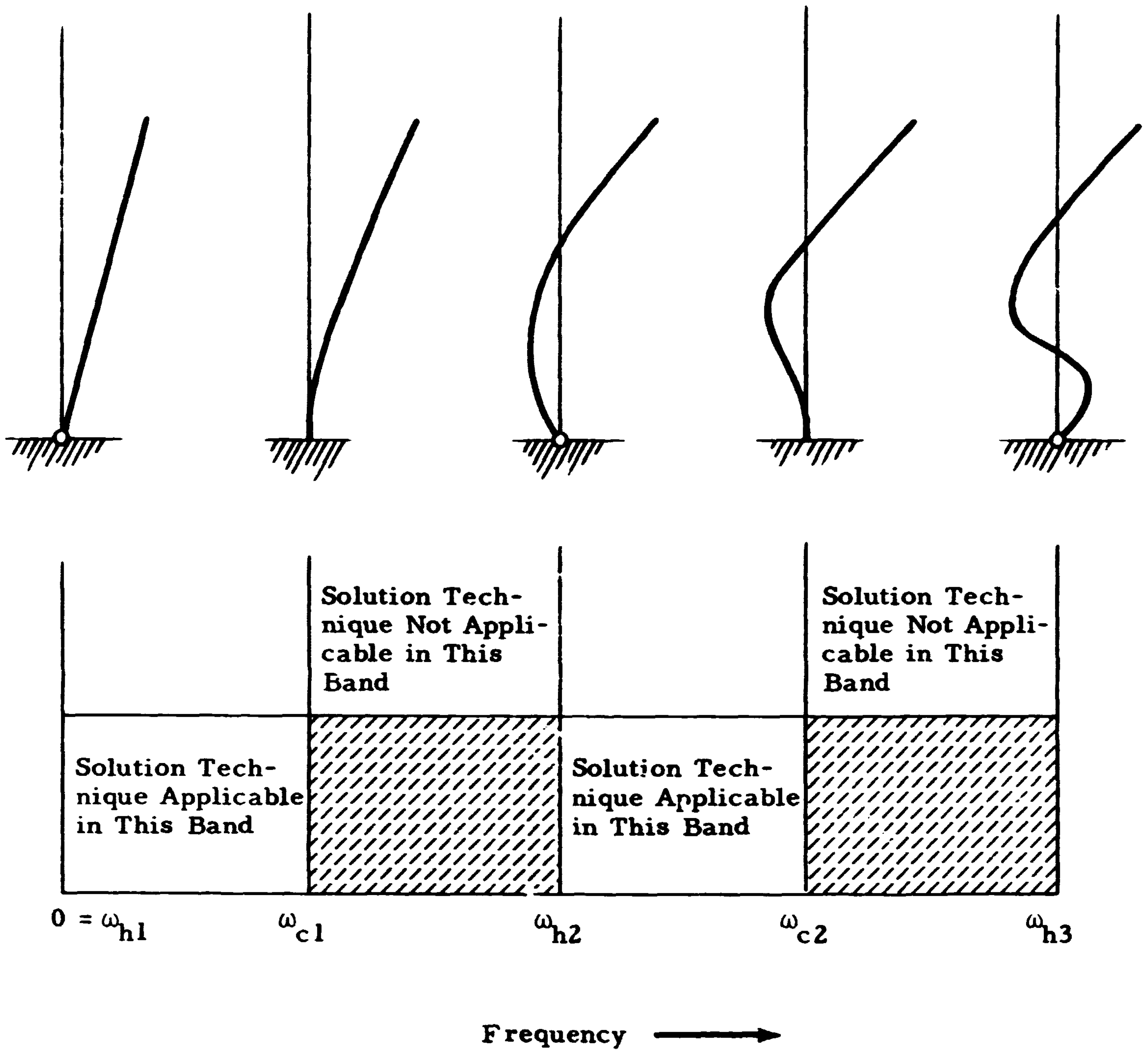

Fig. 2 - Frequency Bands Where Solution Technique is Applicable

The end conditions at $x = 0$ may now be written as

$$EI_o u''_o - \frac{(1 + \alpha^2)}{1 + \alpha/\beta} k_o u'_o = 0 \tag{16}$$

and

$$EI_o v''_o - \frac{1 + \alpha^2}{1 - \alpha\beta} k_o v'_o = 0 \tag{17}$$

where

$$\alpha = \omega c_o / k_o \tag{18}$$

is a measure of the amount of damping. In addition, the relationship

$$u'_o = \frac{\alpha + \beta}{1 - \alpha\beta} v'_o \tag{19}$$

may also be derived. Equations (10), (12) and (17) are the governing equations for the free vibration solution of the beam with an equivalent base stiffness:

$$k = \frac{1 + \alpha^2}{1 - \alpha\beta} k_o \tag{20}$$

The frequency of this free vibration of the equivalent system must be ω, the actual forcing frequency. Consequently, k and β can be determined by matching the natural frequencies of the undamped system with ω. For each ω, there can be no more than one value of k satisfying the above requirement. The out-of-phase component of response, $v(x)$, can therefore be described by a single mode shape function, $\phi_n(x)$, of the undamped beam with a rotational base spring of stiffness k given by Eq. (20). Let $\phi_n(x)$ be normalized with respect to the deflection at $x = \ell$, then

$$v(x) = v_n(\ell)\, \phi_n(x) \tag{21}$$

The magnitude of $v_n(\ell)$ can be determined via energy considerations. Let W denote the work done per cycle of vibration by the forcing function $F(x) \sin\omega t$.

$$W = \int_0^{2\pi/\omega} \int_0^{\ell} F(x) \sin\omega t \frac{\partial}{\partial t} w(x,t)\, dx\, dt$$

$$= -\pi v_n(\ell) F_n \tag{22}$$

where

$$F_n = \int_0^{\ell} F(x) \phi_n(x)\, dx \tag{23}$$

is a functional of the forcing frequency ω because $\phi_n(x)$ varies slightly with ω. The energy dissipated per cycle at the joint at $x = 0$ is

$$D = \int_0^{2\pi/\omega} \left[EI_o \frac{\partial^2}{\partial x^2} w(o,t)\right] \left[\frac{\partial^2}{\partial t\, \partial x} w(o,t)\right] dt$$

$$= \pi EI_o (v_o'' u_o' - u_o'' v_o')$$

In view of Eqs. (15), (17) and (19),

$$D = \pi v_n^2(\ell) \left[\phi_n'(o)\right]^2 \frac{\alpha k_o (1 + \alpha^2)(1 + \beta^2)}{(1 - \alpha\beta)^2} \tag{24}$$

Because $W = D^*$ the right-hand sides of Eqs. (22) and (23) can be equated, and

---

*Damping due to other sources may be conveniently introduced here if necessary.

$$-v_n(\ell) = \frac{F_n(1 - \alpha\beta)^2}{\alpha \left|\phi'_n(o)\right|^2 (1 + \beta^2)(1 + \alpha^2)\, k_o} \tag{25}$$

The following procedures convert the solution into a more familiar format. Let

$$(1 + \alpha^2)\, k_o = k_1$$

From Eq. (20),

$$k = \frac{k_1}{1 - \alpha\beta}$$

So that

$$\beta = \frac{k - k_1}{\alpha k} \tag{26}$$

and

$$\frac{(1 - \alpha\beta)^2}{\alpha(1 + \beta^2)(1 + \alpha^2)\, k_1} = \frac{\alpha k_1}{\left[\alpha^2 k^2 + (k - k_1)^2\right]}$$

The solution for $v_n(\ell)$ can now be written as

$$-v_n(\ell) = \frac{F_n\ \alpha k_1}{\left[\alpha^2 k^2 + (k - k_1)^2\right] \left[\phi'_n(o)\right]^2} \tag{27}$$

The quantity $(k - k_1)$ in the denominator is related to the difference in natural frequencies of the undamped beam. Let $\phi_{n1}(x)$ be the nth mode shape for $\omega = \omega_1$ (where $k = k_1$), and let $\phi_n(x)$ be the nth mode shape at the forcing frequency, ω. The following sets of equations must be satisfied:

$$\rho \omega_{n1}^2 \phi_{n1} - (EI\, \phi''_{n1})'' = 0 \tag{28}$$

with

$$\phi_{n1}(o) = \phi''_{n1}(\ell) = \phi'''_{n1}(\ell) = 0 \tag{29}$$

$$EI_o\, \phi''_{n1}(o) = k_1\, \phi'_{n1}(o) \tag{30}$$

and

$$\rho \omega^2 \phi_n - (EI\, \phi''_n)'' = 0 \tag{28-a}$$

with

$$\phi_n(o) = \phi''_n(\ell) = \phi'''_n(\ell) = 0 \tag{29-a}$$

$$EI_o\, \phi''_n(o) = k\, \phi'_n(o) \tag{30-a}$$

Multiply both sides of Eq. (28) by $\phi_n(x)$, integrate over the length of the beam, and substitute Eqs. (29) and (30) into the result. One obtains the relationship,

$$\omega_{n1}^2 \int_0^{\ell} \rho\, \phi_{n1}\, \phi_n\, dx = k_1\, \phi'_{n1}(o)\, \phi'_n(o) + \int_0^{\ell} EI\, \phi''_{n1}\, \phi''_n\, dx$$

Similar manipulations with Eqs. (28-a), (29-a) and (30-a) yield the result

$$\omega^2 \int_0^{\ell} \rho\, \phi_n\, \phi_{n1}\, dx = k\, \phi'_n(o)\, \phi'_{n1}(o) + \int_0^{\ell} EI\, \phi''_n\, \phi''_{n1}\, dx$$

By eliminating the last integrals in the last two equations and rearranging the required difference relationship between frequency and base stiffness, the following is obtained:

$$\left(\omega^2 - \omega_{n1}^2\right)\int_0^{\ell} \rho\, \phi_n\, \phi_{n1}\, dx = (k - k_1)\, \phi_n'(o)\, \phi_{n1}'(o) \tag{31}$$

By incorporating Eq. (31) into Eq. (27), the solution for the out-of-phase response amplitude is finally obtained in the desired form:

$$-v_n(\ell) = \frac{\dfrac{F_n}{\omega_{n1}^2 \int_0^{\ell} \rho\, \phi_n\, \phi_{n1}\, dx} \cdot \dfrac{\alpha k\, \phi_n'(o)\, \phi_{n1}'(o)}{\omega_{n1}^2 \int_0^{\ell} \rho\, \phi_n\, \phi_{n1}'\, dx} \cdot (1 + \alpha^2)\, \dfrac{\phi_{n1}'(o)}{\phi_n'(o)}}{\left[\dfrac{\alpha k\, \phi_n'(o)\, \phi_{n1}'(o)}{\omega_{n1}^2 \int_0^{\ell} \rho\, \phi_n\, \phi_{n1}\, dx}\right]^2 + \left(1 - \dfrac{\omega^2}{\omega_{n1}^2}\right)^2} \tag{32}$$

A definition for "low joint damping" may conveniently be introduced at this stage of development: if the dashpot strength c_o is such that the quantity

$$\alpha = \frac{\omega c_o}{k_o} < < 1 \tag{33}$$

For the frequency range of concern, the structure joint is said to have low damping. Under this condition the following approximations may be introduced:

$$(1 + \alpha^2) \cong 1 \tag{33-a}$$

$$\phi_n(x) \cong \phi_{n1}(x)\,,\; \phi_n'(x) \cong \phi_{n1}'(x)\,, \ldots \tag{33-b}$$

$$\int_0^{\ell} \rho\, \phi_n(x)\, \phi_{n1}(x)\, dx \approx \int_0^{\ell} \rho\, \phi_{n1}^2(x)\, dx = m_{n1} \tag{33-c}$$

and

$$F_n = \int_0^{\ell} F(x)\, \phi_n(x)\, dx \approx \int_0^{\ell} F(x)\, \phi_{n1}(x)\, dx \tag{33-d}$$

to reduce Eq. (32) to the familiar form for the one-degree-of-freedom system:

$$-v_n(\ell) = \frac{2\zeta_{n1}\frac{\omega}{\omega_{n1}}\,\frac{F_{n1}}{K_{n1}}}{\left(2\,\zeta_{n1}\frac{\omega}{\omega_{n1}}\right)^2 + \left(1+\frac{\omega^2}{\omega_{n1}^2}\right)^2} \tag{34}$$

where

$$K_{n1} = \omega_{n1}^2\ m_{n1} \tag{35}$$

$$\zeta_{n1} = \frac{c_o}{2\,m_{n1}\,\omega_{n1}}\ \left[\phi'_{n1}(o)\right]^2 \tag{36}$$

Note that in each case, the error introduced by the approximations employed to obtain the solution can be computed for a given problem.

At frequencies where $\beta = \pm\ 1$,

$$u''_o = \pm\ v''_o$$

These frequencies, therefore, correspond to "half-power frequencies." The out-of-phase mode shapes are those for the undamped beam, but will base stiffnesses:

$$k_{\pm} = (1 \pm \alpha)\ k_o$$

For "light damping," $\alpha < < 1$, the corresponding mode shapes differ from that at $\omega = \omega_{n1}$ by (calculably) small amounts.

The solution of the in-phase response component, u(x), can be obtained from Eqs. (9), (11) and (13) which are identical to those composed by the forced vibration problem of the undamped beam in Fig. 3.

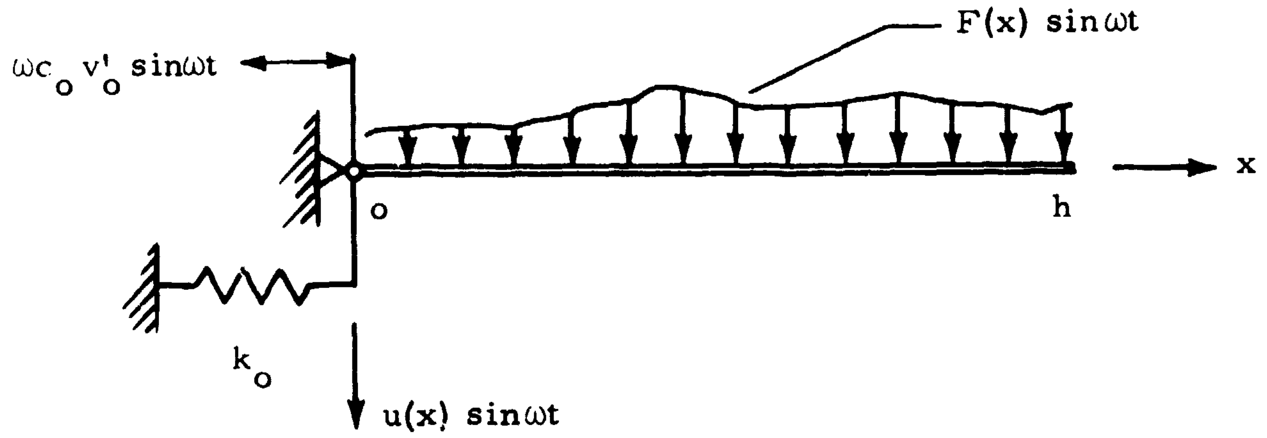

Fig. 3 - Equivalent System for Determining In-Phase Response Component

The end condition at $x = 0$ differs from the original problem in that it is undamped, with a rotational spring rate k_o, and an applied moment, $\omega c_o v'_o \sin\omega t$. Since v'_o is by now a known function of ω and $F(x)$, the solution of this problem, and hence of the in-phase response of the damped beam can be written immediately:

$$u(x) = \sum_{n=1}^{\infty} u_n(\ell)\, \phi_{no}(x) \tag{37}$$

where $\phi_{no}(x)$ are the natural modes of the beam corresponding to the rotational base spring rate k_o, and are normalized to the deflection at $x = \ell$. The generalized forces are

$$f_n = \int_0^{\ell} F(x)\, \phi_{no}(x)\, dx + \omega c_o\, v'_o\, \phi'_{no}(o) \tag{38}$$

In the nth frequency band (defined in Fig. 2),

$$v'_o = v_n(\ell)\, \phi'_n(o)$$

With $v_n(\ell)$ given by either Eq. (25) or (32), the coefficients $u_n(\ell)$ are, therefore, given by the expression

$$u_n(\ell) = \frac{\int_0^\ell F(x)\ \phi_{no}(x)\ dx + \omega c_o\ v_n(\ell)\ \phi_n'(o)\ \phi_{no}'(o)}{\left(\omega^2 - \omega_{no}^2\right) \int_0^\ell \rho\ \phi_{no}^2(x)\ dx} \tag{39}$$

In particular, when $\omega = \omega_{no}$, the equation governing the out-of-phase response indicates that k, the equivalent spring rate, is equal to the actual spring rate, so that, from Eq. (20), $\beta = -\alpha$. Equation (25) then yields,

$$v_n'(\ell) = -\frac{F_{no}}{\alpha k_o\ \phi_{no}'(o)}$$

Therefore, the generalized force, f_n, of the above forced vibration problem vanishes for all natural frequencies of the undamped beam.

Equation (39), of course, is identical to the familiar in-phase modal response of the beam with a modal damping coefficient of

$$\zeta_n = \frac{c_o\ \phi_n'(o)\ \phi_{no}'(o)}{2 m_n\ \omega_n} \tag{40}$$

for all values of dashpot strength, c_o.

Equations (32) and (39) are general solutions of the vibration of a beam with an end dashpot. For the case of low joint damping, the simplified solution form of Eq. (34) may be used. The errors introduced are associated with the approximations shown in Eqs. (33-a), (33-b), (33-c) and (33-d). The approximate solution is identical in form to the solution of a single degree-of-freedom system.

The properties T and ϕ of the hysteresis integral, Eq. (7), are to be such that the energy dissipates per cycle, D, is independent of the frequency, and is proportional to the square of the amplitude of the rotation at the end x = 0. Then

$$D = \int_0^{2\pi/\omega} \frac{\partial}{\partial t} w'(o,t) \bullet gH\left[w'(o,t)\right] dt = \pi g (u_o'^2 + v_o'^2) \int_0^T \varphi(\tau) \sin\omega\tau \, d\tau \tag{41}$$

Therefore, T and ϕ must be such that

$$\int_0^T \phi(\tau) \sin\omega\tau \, d\tau = h, \text{ a constant} \tag{42}$$

which also implies that

$$\int_0^T \phi(\tau) \cos\omega\tau \, d\tau = 0 \tag{43}$$

Substituting Eq. (8) into Eq. (6), the hysteretic boundary condition at x = 0, and applying Eqs. (42) and (43),

$$EI_o \, u_o'' - k\, u_o' + g\, h\, v_o' = 0 \tag{44}$$

$$EI_o \, v_o'' - k\, v_o' - g\, h\, u_o' = 0 \tag{45}$$

The solution for the beam with a hysteretic boundary condition is therefore the same as that for a beam with a viscous damper, having an equivalent dash-pot strength of

$$c' = g\, h/\omega \tag{46}$$

Nonlinear hysteretic damping is represented differently. The linear analysis shown above, however, serves the purpose of demonstrating that, conceptually, hysteresis can be analyzed in a manner similar to that for viscous damping.

2.2 GENERAL MODAL RESPONSES

In the technique employed in the last section, the critical step is to determine the deflection shape of the out-of-phase response component. Other steps follow naturally. For the beam with a single-end damper, the out-of-phase deflection shape varies with frequency; the higher the dashpot strength, the greater the rate of variation with frequency. For the case of low-joint damping, it has been shown that the undamped mode shape of the beam can be used for all frequencies near each resonance. For the general case in which a simple, continuous substructure or structural element with a damper at each end and with distributed damping (such as linear material damping), similar conclusions can undoubtedly be reached by purely theoretical considerations. The following analytical approaches are, however, suggested without theoretical proof. They must be considered as propositions to be verified experimentally or via numerical analyses for individual structures.

The steady-state response of a simple structure with a small amount of distributed non-proportional damping and dissipative boundary conditions can be estimated by assuming that the deflection shape of the out-of-phase response component is the same as the undamped structure. The amplitude of this response can be estimated by equating the total rate of energy dissipation to the rate of work being done by the external excitation, using the assumed deflection shape for computing both rates. Furthermore, the resulting solution for the steady-state vibration will be used to construct the modal equation of motion for other types of excitation, with modal coefficients specified by the characteristics of the steady-state response.

For structures with high, non-proportional damping, this approach can still be used, but with an iterative procedure. The undamped mode shape is used initially and the corresponding energy dissipation rate then computed.

Equivalent dissipative boundary conditions which dissipate energy at the same rate as the non-proportional part of the distributed damping are then hypothesized. An improved deflection shape is then computed according to the technique introduced in the previous section. The process is repeated until no significant differences are observed between two successively computed deflection shapes. In all cases, undamped mode shapes are used for the in-phase response component.

Although relatively general concepts concerning non-proportional damping can be visualized after a simple, representative problem has been considered, nonlinear damping is a different matter. To start with, a separable solution of the form given in Eq. (8) for the simple beam problem cannot be found if one of the boundary conditions is nonlinear (conservative or dissipative). Solutions of the response of a simple, continuous system with nonlinearities probably can be obtained only by numerical techniques. If numerical solution techniques are to be used, extensive parametric studies must be conducted beforehand to provide enough information for developing experimental approaches that are flexible enough to measure damping properties of arbitrary characteristics.

In view of the previous conclusion that the steady-state response solutions of a simple structure with non-proportional damping have the same general forms as those obtained by assuming proportional damping, a nonlinear modal equation is postulated to handle nonlinear damping and stiffness. This equation will, in the limit, yield the correct linear solution. Since the nonlinear term introduced can be left general, it is expected to be sufficiently flexible for developing experimental approaches.

2.3 FUNDAMENTAL SOLUTIONS OF NON-LINEAR MODAL VIBRATIONS

The equation of motion for the non-linear steady-state modal responses of the beam can now be written as

$$M\ddot{Z} + KZ + f(Z, \dot{Z}) = F \sin \omega t \tag{47}$$

where Z is the modal response, M the generalized mass, $F(t)$ the generalized force, KZ the linear component of the restoring force, and $f(Z, \dot{Z})$ the non-linear modal restoring force including dissipative components. For the beam with end damping analyzed in Section 2, Z may be considered as the tip deflection in the n^{th} mode.

Experimentally, sinusoidal tests are desirable because test signals are easily generated and precisely controlled. Furthermore, the fundamental frequency component of the response contains information for reconstructing the unknown function $f(Z, \dot{Z})$.

Assume

$$Z = z \sin\left|\omega t - \theta(\omega)\right| \tag{48}$$

Substituting it into Eq. (47), the following expressions are obtained:

$$(K - M\omega^2)\, z + f_s(z, \omega z) = F \cos\theta \tag{49}$$

and

$$f_c(z, \omega z) = F \sin\theta \tag{50}$$

where

$$f_s = \frac{1}{\pi}\int_0^{2\pi/\omega} f(Z, \dot{Z}) \sin(\omega t - \theta)\, dt \tag{51}$$

and

$$f_c = \frac{1}{\pi}\int_0^{2\pi/\omega} f(Z, \dot{Z}) \cos(\omega t - \theta)\, dt \tag{52}$$

A discussion of the above approach is summarized in Ref. 2 for a variety of functions $f(Z, \dot{Z})$. A similar analysis for a class of hysteresis damping is found in Ref. 3.

The in-phase component of $f(Z, \dot{Z})$ is found to be zero for a general non-linear viscous damping force, i.e., if

$$f(Z, \dot{Z}) = \dot{Z} \sum_{i=0}^{I} C_i \, |\dot{Z}|^i \tag{53}$$

then

$$f_s = 0 \tag{54}$$

Also, for a hysteretic damping force

$$f(Z, \dot{Z}) = C \frac{\dot{Z}}{|\dot{Z}|} h(Z) \tag{55}$$

$$f_s = f_s(z), \tag{56}$$

If the definition

$$\lim_{\dot{Z} \to 0} \frac{\dot{Z}}{|\dot{Z}|} = 0, \quad \text{independent of the direction of approach} \tag{57}$$

is adopted, or if the sign function in Eq. (55) is replaced by the function, $g(\dot{Z})$, shown in Fig. 4, the structure will be statically linear but dynamically non-linear, as had been observed for real structures. If $g(\dot{Z})$ is used, the in-phase component of $f(Z, \dot{Z})$ will be practically independent of frequency, i.e.,

$$f_s \cong f_s(z) \tag{58}$$

for ω greater than a certain lower limit determined by the point $\underline{\dot{Z}}$ in Fig. 4.

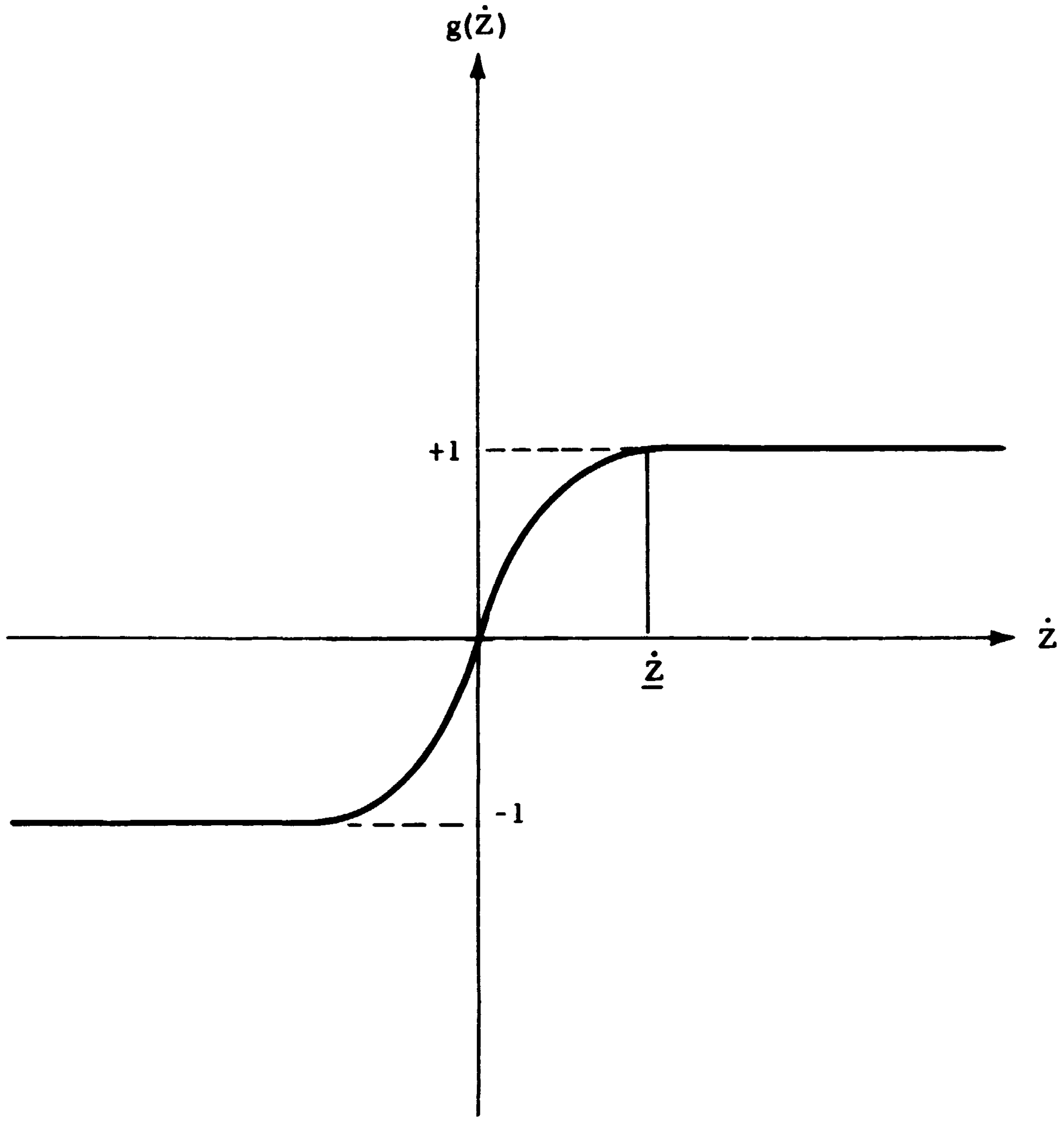

Fig. 4 - The Function $g(\dot{Z})$

Section 3
EXPERIMENTAL APPROACH

3.1 TEST PHILOSOPHY

The principal objective of the type of dynamic tests being conducted in this study is to determine damping (and related) properties of substructures and structural components with internal and boundary damping. As in all property – determination experiments, the number of assumptions concerning the specimen behavior must be kept to a minimum. For substructural testing, assumptions are limited to the following:

- The specimen may be physically separated from a complex structure, and the boundary conditions in the test setup are identical to those in the structure.
- The test frequency and response amplitude of the test specimen may be varied to cover those expected of the specimen while it is an integral part of the entire structure. The deformation should also closely approximate the in situ deformation shape.
- Environmental effects are controllable and can be isolated from test results.

These assumptions do not exert insurmountable test constraints. For example, masses can be added to the specimen to lower the resonant frequencies of the specimen until the lowest mode is close to the "resonant frequencies" of the entire structure. Large amplitudes of the specimen are then obtainable at those frequencies with reasonable excitation amplitudes. Environmental conditions are always more easily controlled for the substructure than for the entire structure because of size.

3.2 SELECTION OF TEST EXCITATION MODE

Sinusoidal test excitation is by far the most desirable because

- Data analyses are based on fewer assumptions, and
- Greater test control and data acquisition accuracies are achievable in the steady-state tests than in transient or random vibration tests.

3.3 TEST MEASUREMENTS

Measurable variables are:

- Excitation as a function of time and in particular, concentrated sinusoidal excitation amplitudes can be measured to an accuracy of approximately 1%. Excitation frequency can be held constant and read without difficulty to better than one part in 10^4.
- Responses (displacement, strain, velocity, and acceleration) can be measured to the same degree of accuracy as the excitation. With a tracking bandpass filter, the fundamental frequency component of the response can also be measured with equal accuracy.
- The phase relationship between excitation and fundamental frequency component of response signals should be measurable to an accuracy of $\pm$ 0.5 deg with an electronic phase meter.

3.4 TEST METHOD

Based on theoretical results discussed in Section 2, the analytical procedure to predict structural responses can be considerably simplified if nonproportional damping is low. Experimental procedures can be correspondingly simplified. The first and very important step in a test program is, therefore, to estimate the magnitude of the nonproportional part of damping. Conversely, an indicator parameter which gives qualitative descriptions of the amount of nonproportional damping is the variation of the out-of-phase deflection over the -3 dB (from peak response) frequency band for each resonance. The integral

$$\int_0^{\ell} \rho \, \phi_n(x) \, \phi_{n1}(x) \, dx = M_n \tag{59}$$

can be computed. If little variation in M_n is observed over the -3 dB frequency band of a resonance, the leading coefficient of Eq. (47) may be considered frequency independent, and simplified test procedures and subsequent data analyses can be employed. If the out-of-phase deflection shape varies significantly over the -3 dB frequency band, $\phi_n(x)$ should be measured for several frequencies in the steady-state test so that M and other coefficients in Eq. (47) may be determined as functions of the forcing frequency.

In many instances, static calibrations of specimens will show a linear force-deformation relationship; while dynamically, the responses often indicate nonlinearily between resonant excitation and response amplitudes. In addition to nonlinear damping forces (which are the principal cause of nonlinear resonant responses), nonlinear dynamic restoring forces are usually present also, introducing variation of resonant frequencies. Referring to Eq. (49), the frequency at which $\theta = 90$ deg (defined as the resonant frequency in the report, and denoted by ω_1) is governed by the relationship

$$(K - M\omega_1^2) \, z_1 + f_s(z_1) = 0.^* \tag{60}$$

Since ω_1 and z_1 are measurable quantities, the above equation serves to define $f_s(z_1)$. More precisely, the last equation can be written as

$$\frac{1}{M} \, f_s(z_1) = - \left[\bar{\omega}_1^2 - \omega_1^2 \, (z_1) \right] z_1 \tag{61}$$

where

$$\bar{\omega}_1^2 = \omega_1^2 \, (0) = \frac{K}{M} \tag{62}$$

---

*According to previous discussions, the restricted form: $f_s = f_s(z)$ can be used if the damping force is either nonlinear viscous, or hysteretic in nature.

is determined by extrapolating the curve $\omega_1(z_1)$. If, for example, ω_1 is independent of the response amplitude, i.e., if $\omega_1 = \bar{\omega}_1$ for all z_1, then $f_s(z_1) = 0$, and the restoring force is linear.

The coefficient M in Eq. (47) can also be determined experimentally. If non-proportional damping is low, M is a constant. From Eq. (49) it is seen that by testing at a second phase angle, θ_2, over a range of excitation and response amplitudes, the relationship

$$\left[K - M\omega_2^2(z_2)\right] z_2 + f_s(z_2) = F_2(z_2)\cos\theta_2 \tag{63}$$

may be used for this purpose. The functional form of $f_s(z)$ has already been established by the 90-deg test. From Eq. (61)

$$\frac{1}{M} f_s(z_2) = -\left[\bar{\omega}_1^2 - \omega_1^2(z_2)\right] z_2 \tag{64}$$

Combining Eqs. (62), (63) and (64), the following is obtained

$$\left[\bar{\omega}_1^2 - \omega_2^2(z_2)\right] z_2 - \left[\bar{\omega}_1^2 - \omega_1^2(z_2)\right] z_2 = \frac{F_2(z_2)\cos\theta_2}{M}$$

or,

$$\left[\omega_1^2(z_2) - \omega_2^2(z_2)\right] z_2 = \frac{F_2(z_2)\cos\theta_2}{M} \tag{65}$$

In Eq. (65), the quantity $\omega_1(z_2)$ is the function ω_1 evaluated at z_2 and, therefore, is known. Thus, M is determined by

$$M = \frac{F_2(z_2)\cos\theta_2}{\left[\omega_1^2(z_2) - \omega_2^2(z_2)\right] z_2} \tag{66}$$

If non-proportional damping is high, the above test should be repeated over a range of frequencies, each test run at a different phase angle between response and excitation.

The out-of-phase component of $f(Z, \dot{Z})$ in steady-state tests provides measurements of damping. At resonance, this component is given by the relationship

$$f_c(z_1, \omega_1 z_1) = F_1(z_1) \tag{67}$$

The function $f(Z, \dot{Z})$ can be established after f_s and f_c are determined from experimental data in the manner described above. The entire test and data analysis procedure is demonstrated in Section 4.

Section 4
EXPERIMENTAL STUDIES OF A STRUCTURAL MODEL

4.1 TEST OBJECTIVES AND SPECIMEN DESCRIPTION

The objective of the test is to investigate the feasibility of testing substructures and structural elements to obtain basic structural properties and to investigate practical difficulties of the approach.

The test specimen is a 1/5-scale structural model of the Saturn SA-1 launch vehicle. A detailed description of this model is found in Ref. 4. Only the booster stage was used in this experimental program. The center LOX tank was vertically cantilevered to ground via the thrust structure and was tested first. This test configuration is referred to in this report as Configuration I. (See Fig. 5.) An outer LOX tank was then added to the specimen and identical tests were conducted. This setup is defined as specimen Configuration II, (Fig. 6). A second outer LOX tank was later added, and the tests were repeated. This is Configuration III, (Fig. 7).

Referring to Fig. 5, Configuration I is represented by the problem analyzed in Section 2.1. Equivalent rotational stiffness and damping of the base were determined by steady-state tests and analysis of the center LOX tank in the cantilevered configuration. Properties of the outer LOX tanks and spider-beam combination were determined by testing Configurations II and III.

4.2 ANALYSES

The undamped vibrational characteristics of the specimen in the three test configurations were obtained by the use of a digital computer program. Mathematical modeling of each configuration is shown in Figs. 8a, 8b or 8c. The undamped vibrational characteristics are obtained by ignoring the dashpots.

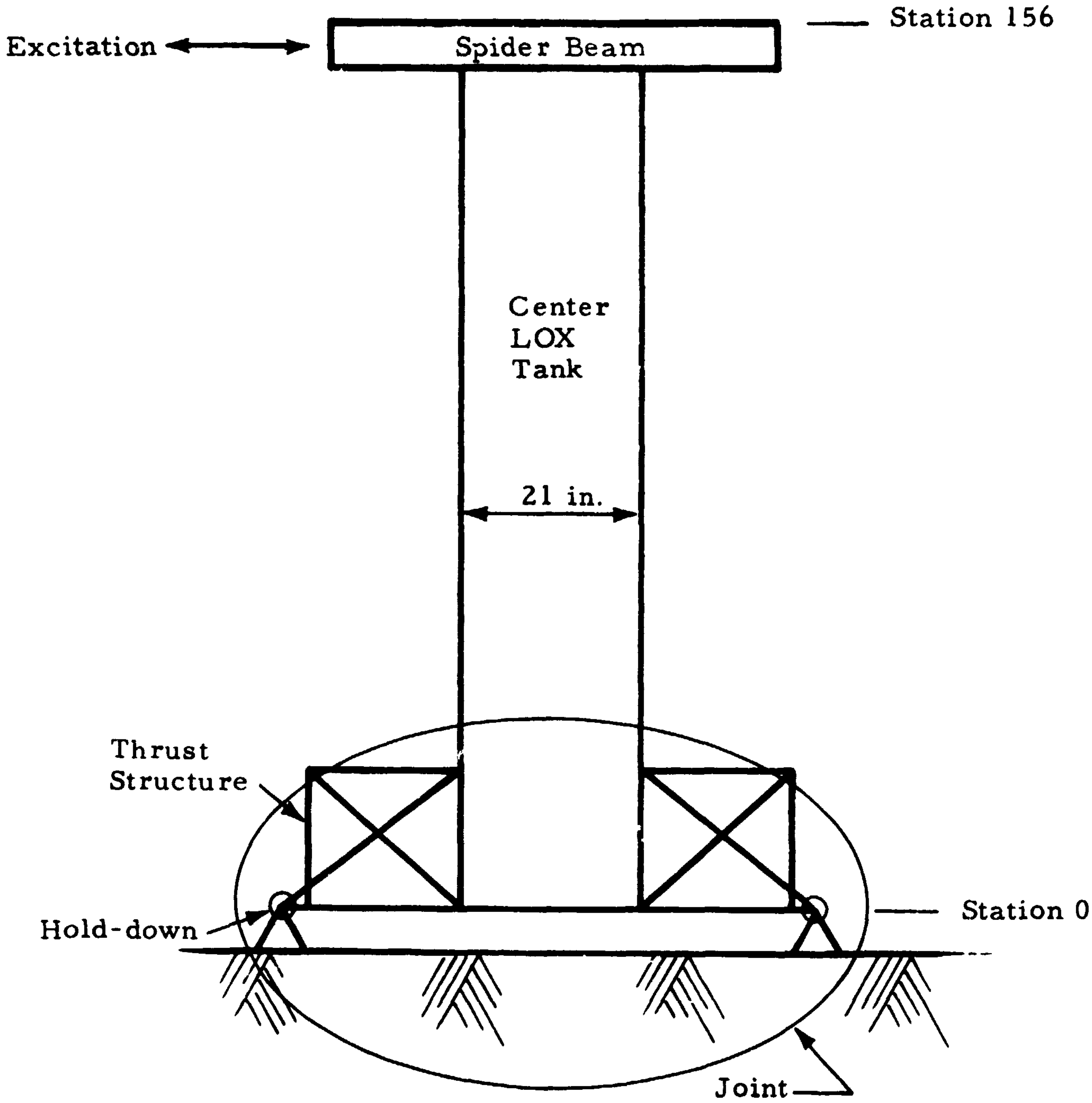

Fig. 5 - Test Configuration I (1/5-Saturn I Model, Center LOX Tank Only)

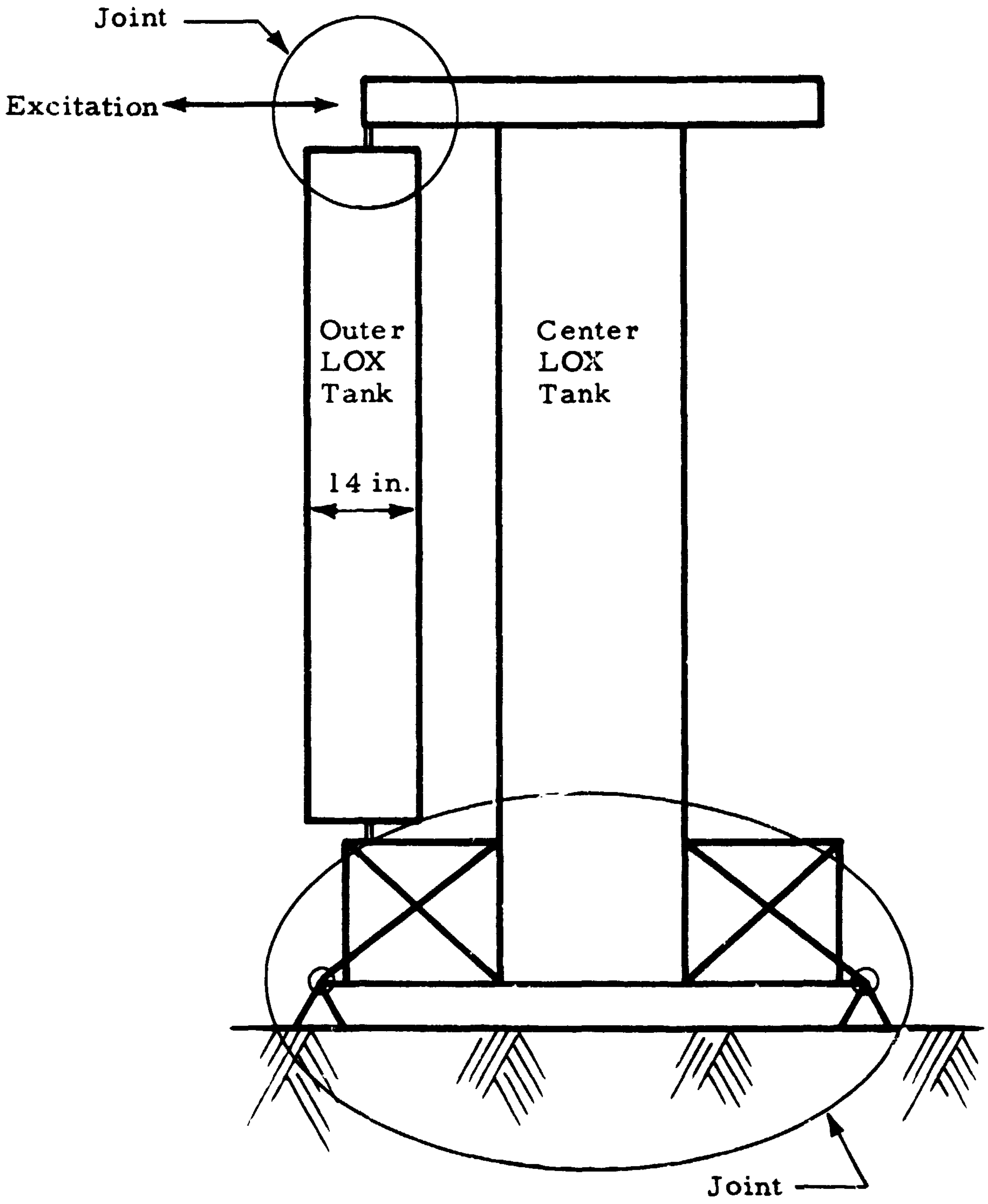

Fig. 6 - Test Configuration II

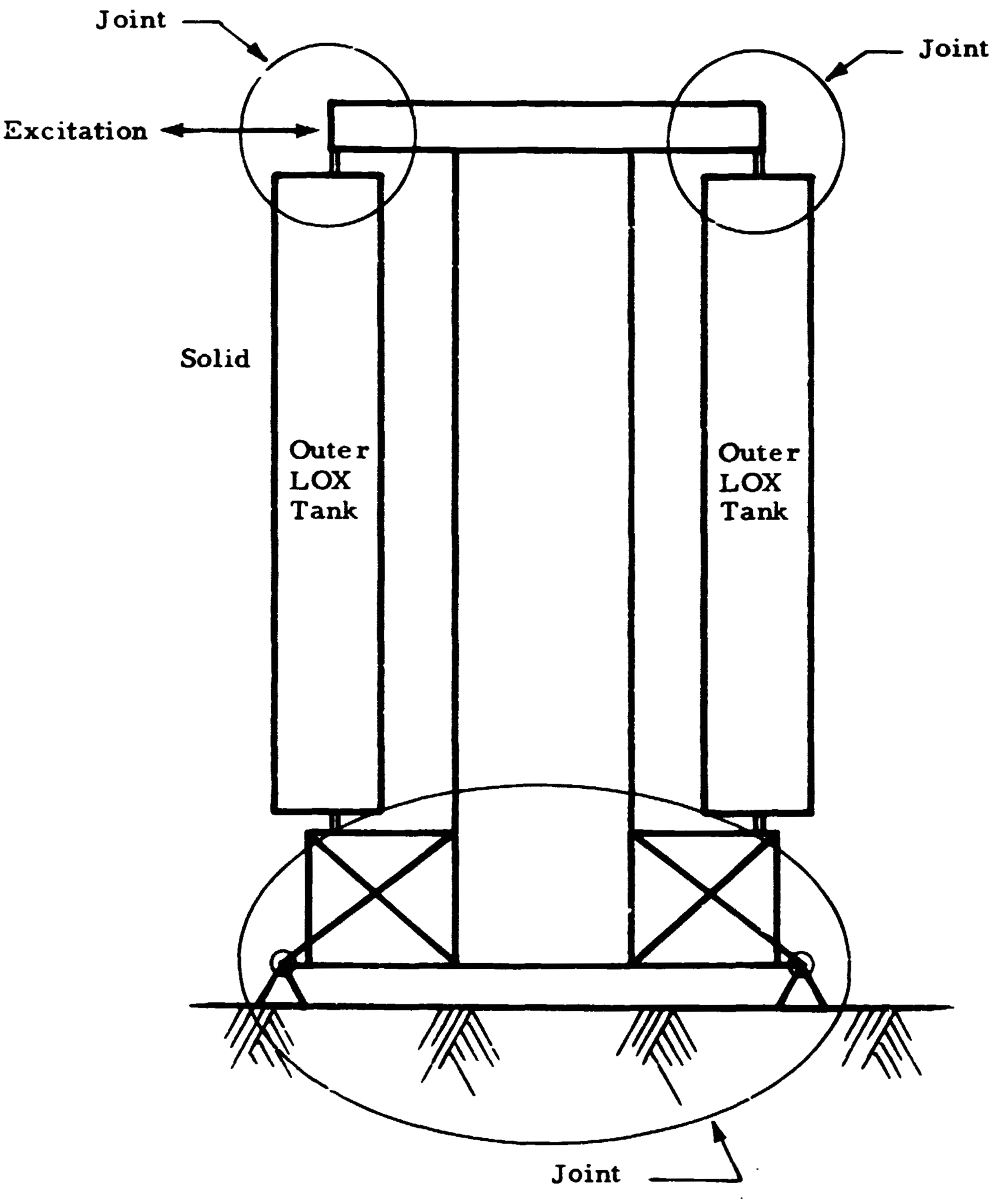

Fig. 7 - Test Configuration III

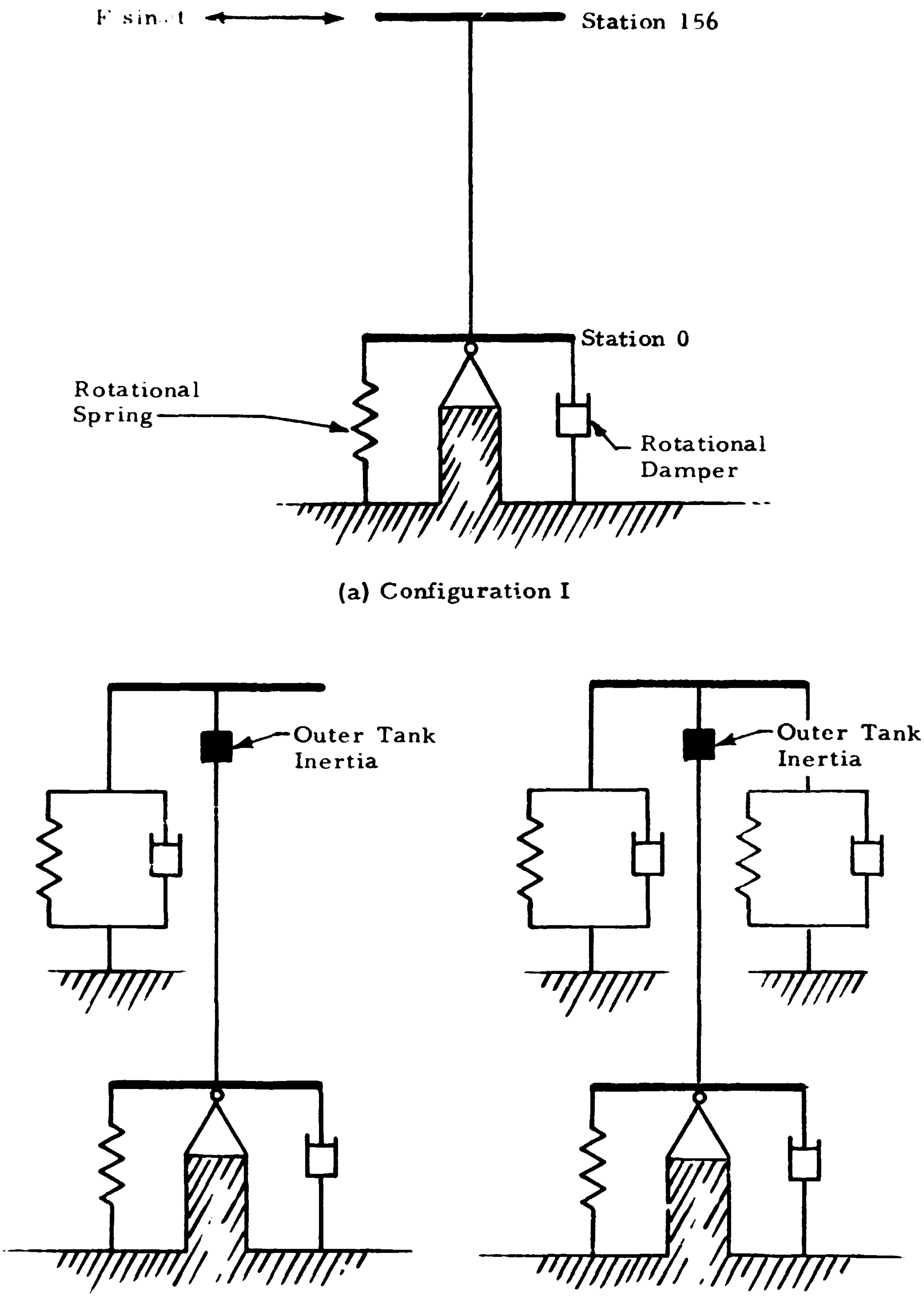

(a) Configuration I

(b) Configuration II

(c) Configuration III

Fig. 8 - Modeling of Test Specimen

The mass and stiffness data for the structure are shown in Figs. 9a, 9b and 9c. Instead of depending completely on analyses, the base and spider-beam stiffnesses were determined by using a combined analytical and experimental approach. Configuration I was analyzed for a range of base stiffnesses first so that curves can be obtained (Figs. 10a and 10b) for the first two undamped natural frequencies as functions of the base stiffness. Experimentally, these frequencies were determined as limits of the 90-deg phase-shift frequencies as the response amplitudes were made to approach zero. The base stiffness giving the correct frequencies is the required value. With an experimentally determined first mode natural frequency of 13.91 Hz, the base stiffness was determined to be 1.10×10^8 in-lb/radian. The calculated second mode frequency for this base stiffness was 115.1 Hz; the measured value was 113.9 Hz.

After the base stiffness had been determined, the equivalent rotational stiffnesses of the outer LOX tank-spider beam combination was determined by similar procedures, using test configurations II and III. The equivalent rotational spring due to one outer LOX tank was found to be 5.94×10^6 in-lb/radian, corresponding to a first mode frequency of 14.82 Hz, (Fig. 10c). For two outer LOX tanks, the stiffness is 11.96×10^6 in-lb/rad, corresponding to a first mode frequency of 15.17 Hz, (Fig. 10d). Table 1 summarizes the calculated characteristics of the three test configurations.

Table 1

Configuration	Mode No.	Natural Freq. (Hz)	Generalized Mass ($lb\text{-}sec^2/in$)	Base* Bending Moment (in-lb)
I	1	13.91	0.191	1.68×10^5
	2	113.9		
II	1	14.82	0.218	1.75×10^5
III	1	15.17	0.245	1.79×10^5

*At Station 37.34 for one-inch tip deflection amplitude

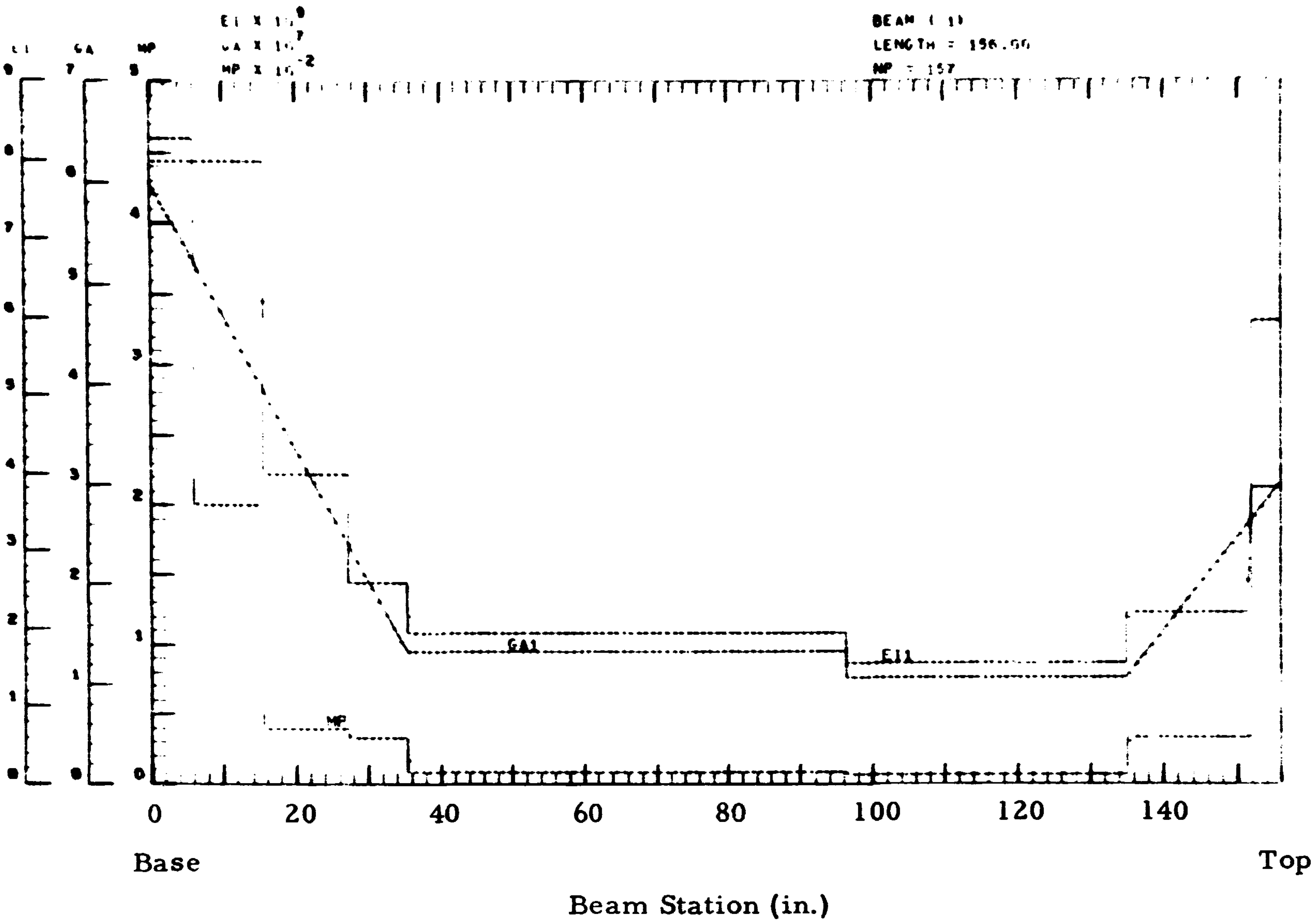

Fig. 9a - Input Data, Configuration I

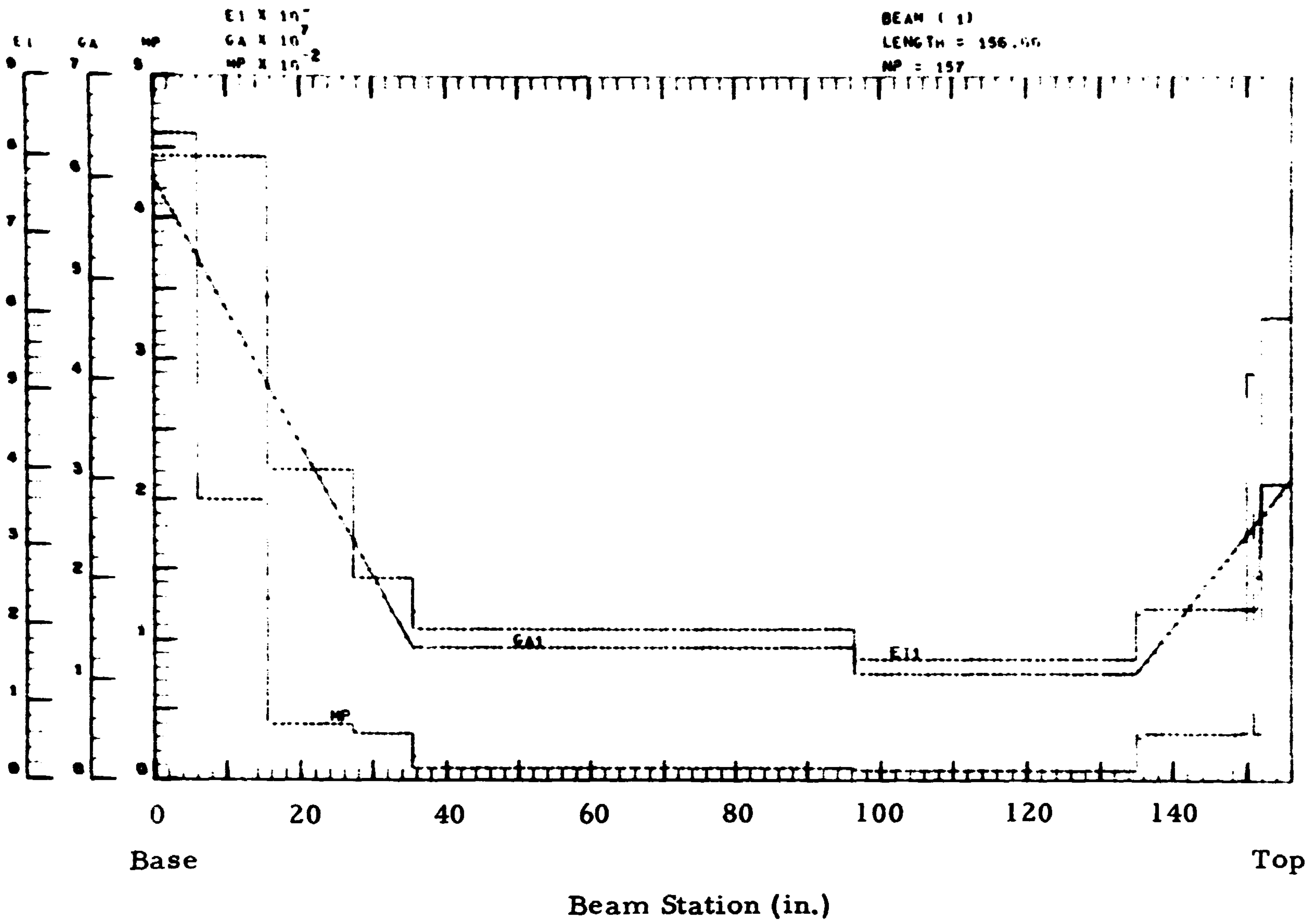

Fig. 9b - Input Data, Configuration II

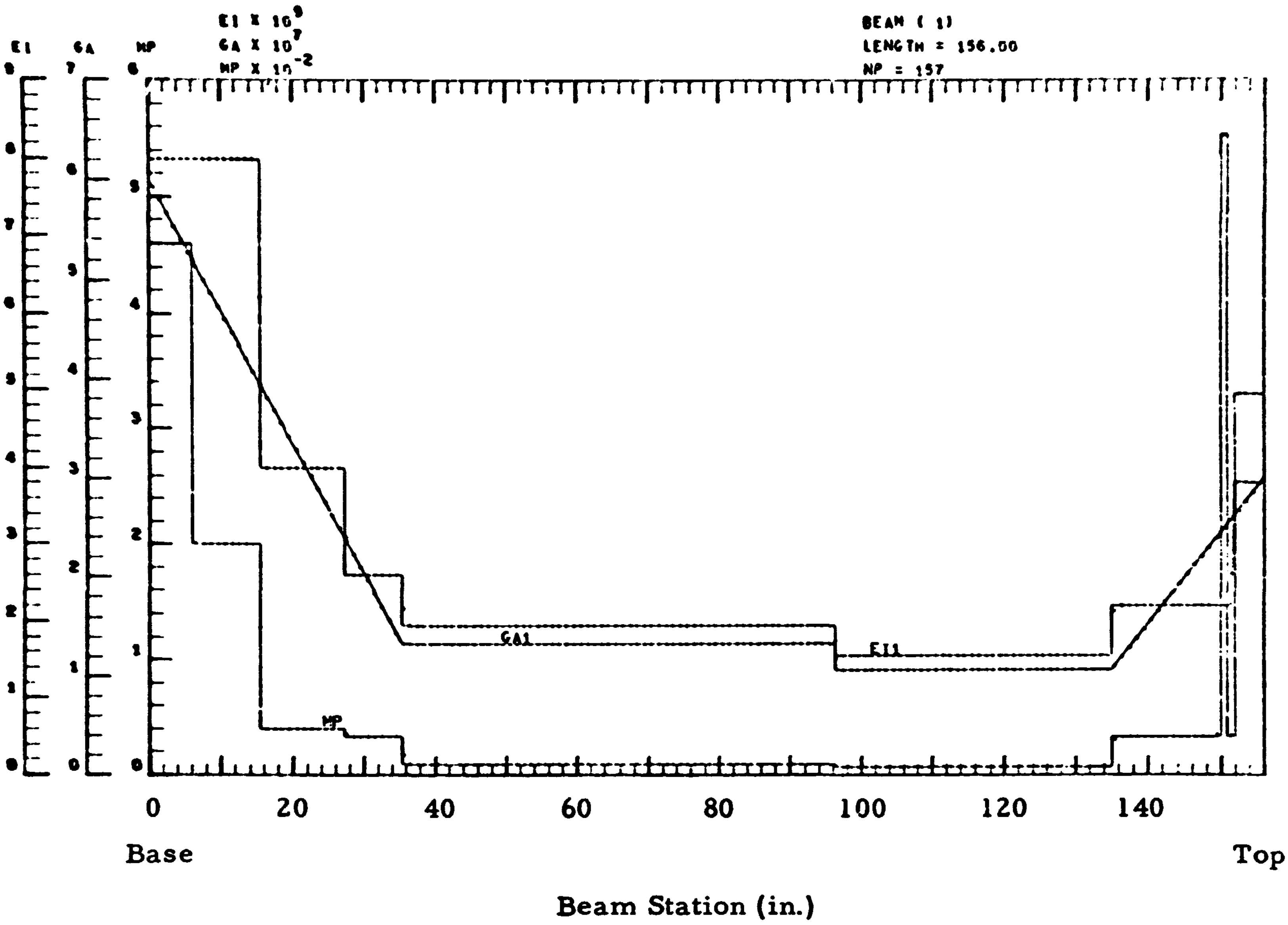

Fig. 9c - Input Data, Configuration IV

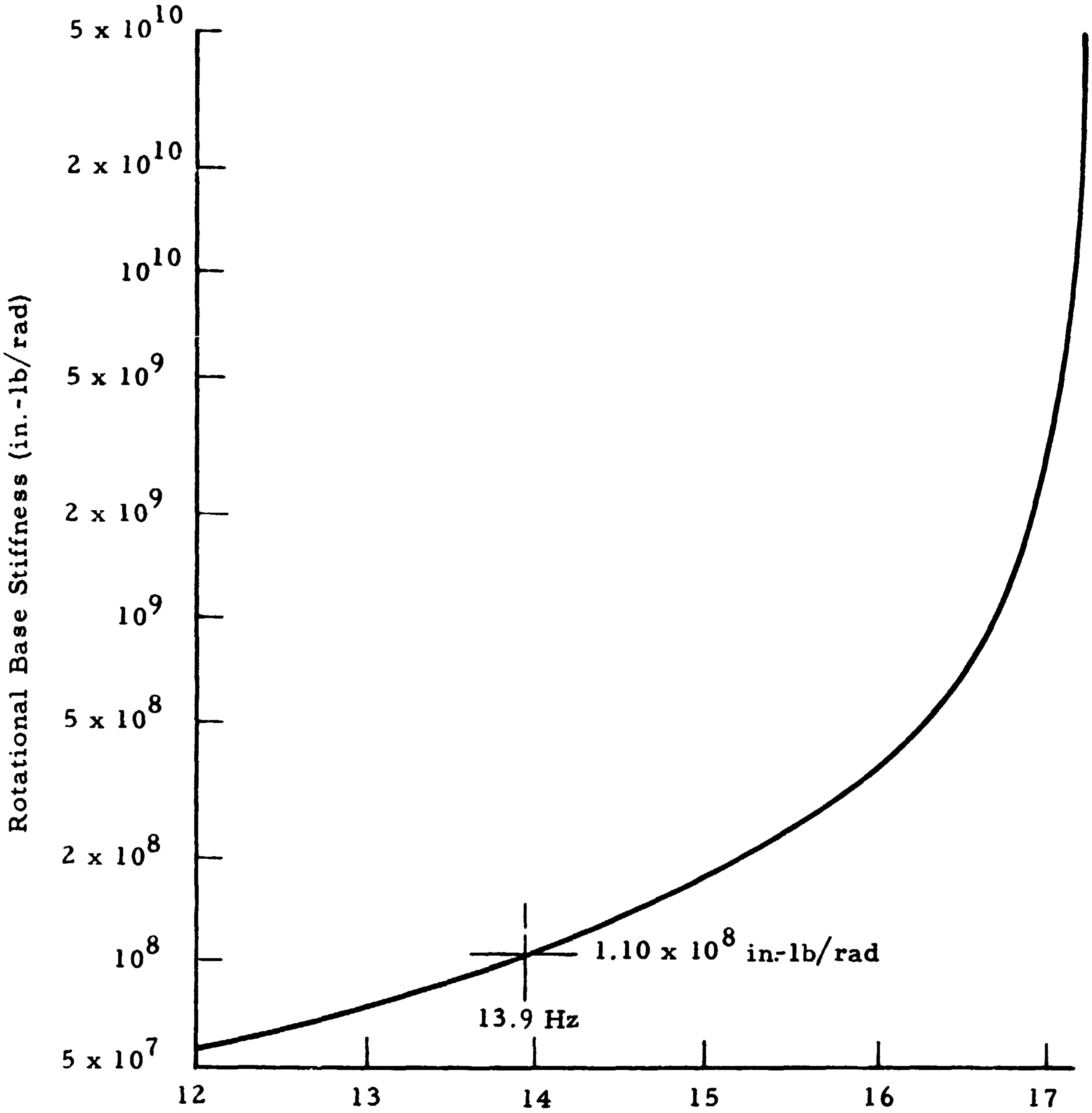

Fig. 10a - Calculated First Mode Natural Frequency vs Base Stiffness (Configuration I)

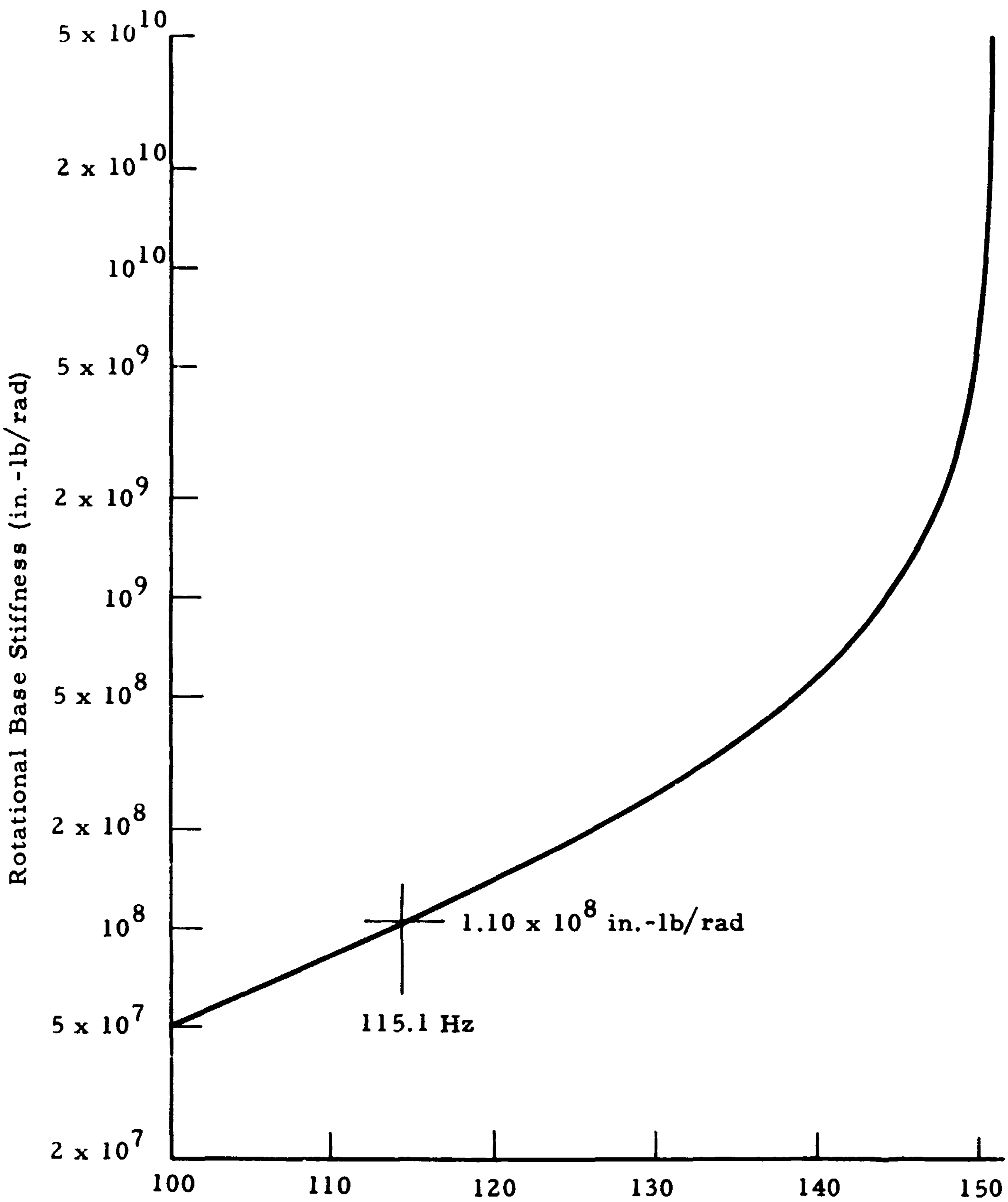

Fig. 10b - Calculated Second Mode Natural Frequency vs Base Stiffness (Configuration I)

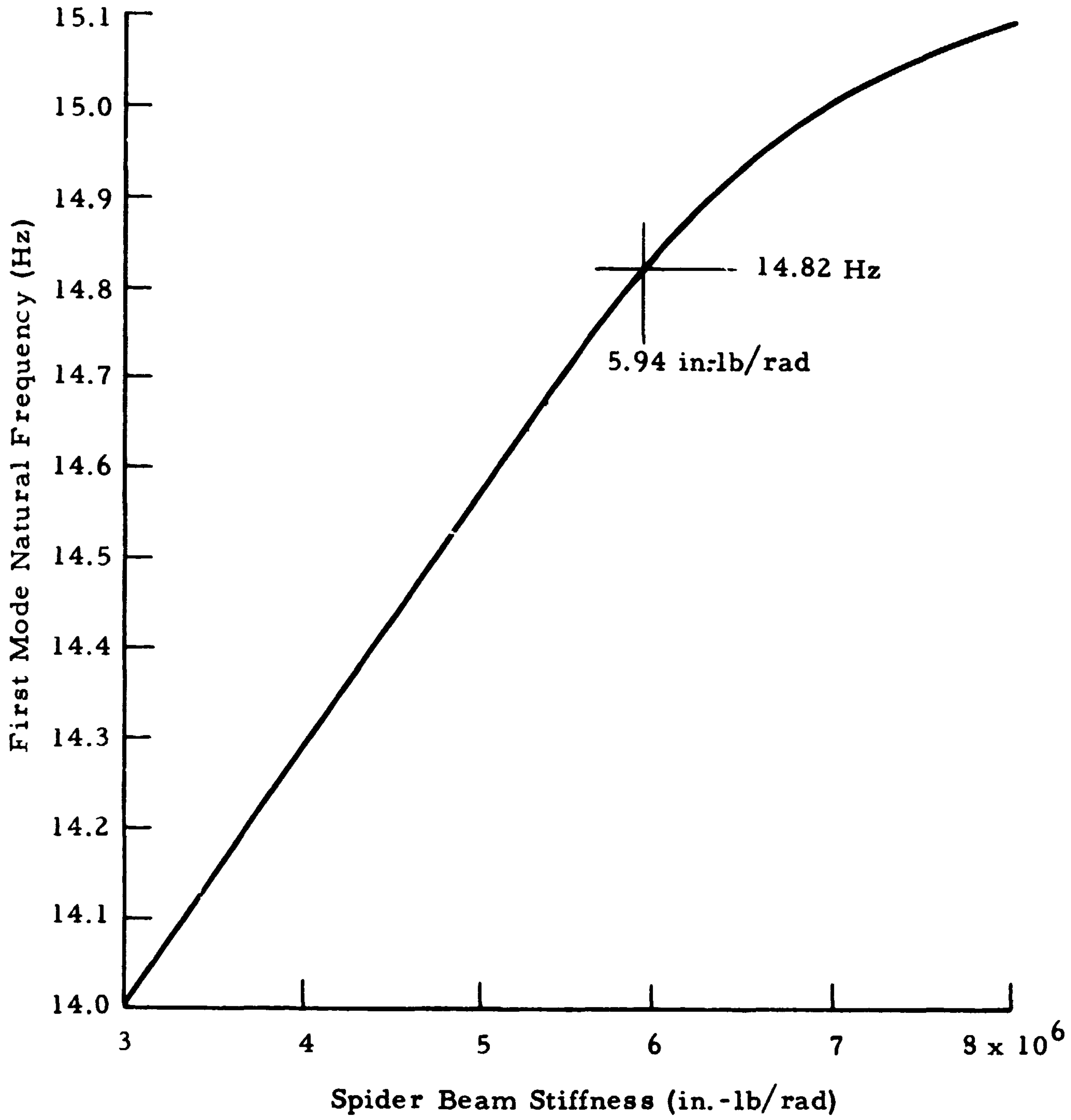

Fig. 10c - Calculated First Mode Natural Frequency vs Spider Beam Stiffness (Configuration II)

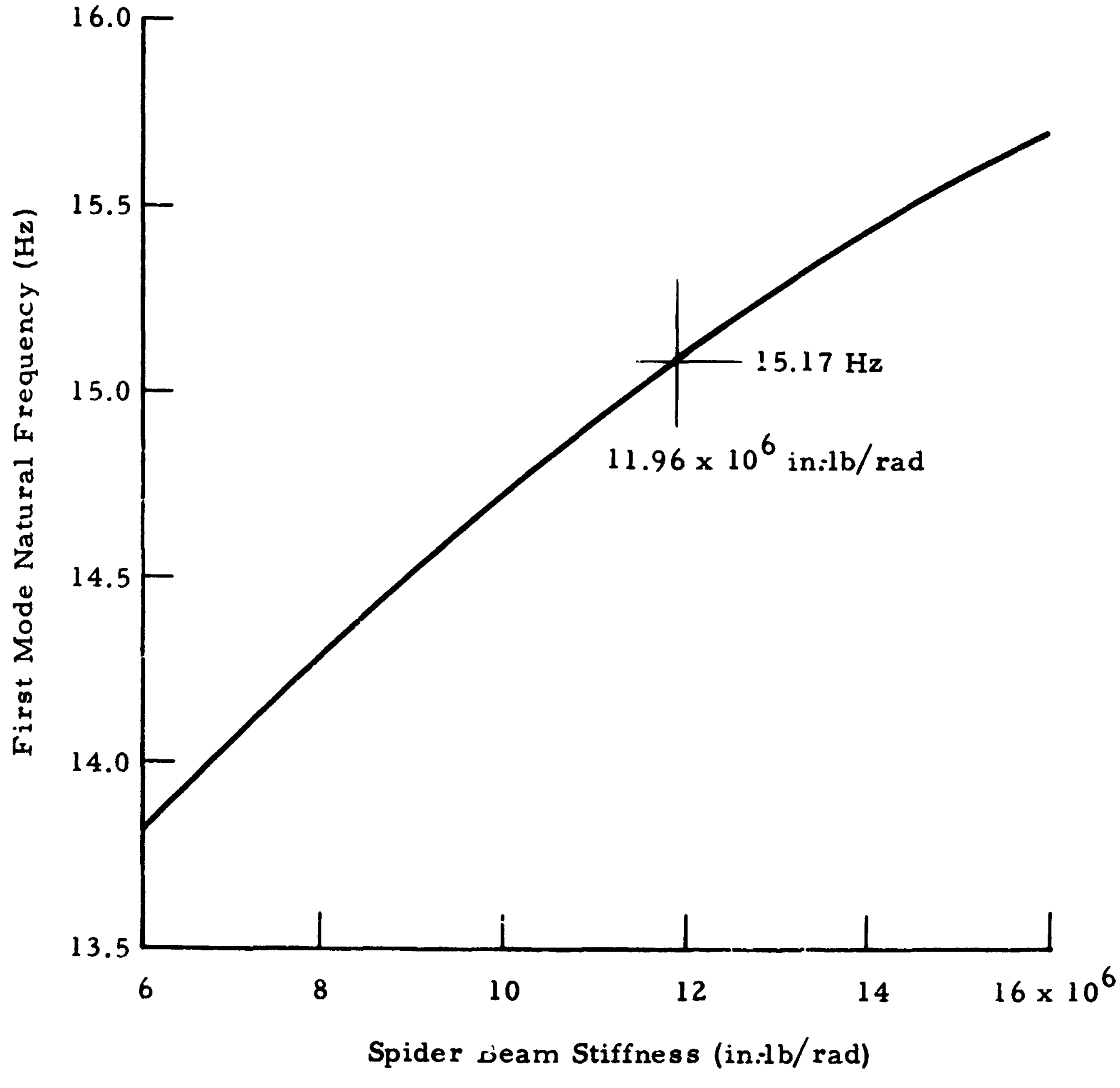

Fig. 10d - Calculated First Mode Natural Frequency vs Spider Beam Stiffness (Configuration III)

Calculated modal characteristics are shown in Figs. 11a through 11f.

4.3 TEST SETUP

Steady-state sinusoidal tests were performed. A single permanent magnet shaker located at mid-spider-beam level provided test excitation. A dc coupled power amplifier was used to drive the shaker. The applied force was measured by a piezoelectric force transducer (sensitivity: 25.3 picocoulombs/lb). The current in the shaker coil was used as the reference signal for phase angle measurements. Specimen response was measured by a solid state strain gage type accelerometer at the point of excitation, and by two metal-foil strain gage bridges located 37.34 in. and 132.90 in. above the base. The strain gages measure bending strains only. The accelerometer is factory-calibrated (3.56×10^{-6} volts/g at ± 2.5 volts excitation). The strain gage bridges were calibrated by applying lateral forces at a height 181 in. above the base of the specimen. Calibration results are shown in Figs. 12a and 12b. These calibrations show that in Configuration I, the specimen is statically linear.

The excitation signal was generated by a voltage-controlled oscillator which has a measured short term drift of one part in 10,000. The excitation frequency was measured with an electronic period timer. The fundamental amplitudes were measured by two simultaneous tracking filters. These tracking filters also perform amplitude detection. Amplitude information was read with a 4-digit digital voltmeter. The tracking filters were adjusted before each test so that they introduced zero phase shift between input and output for the test frequency range. Phase relationship between the shaker current and fundamental response signal was measured with an analog phase meter having an accuracy of $\pm 0.6^{\circ}$ from 10 Hz up. The input signal amplitudes applied to the phase meter were adjusted and maintained constant for each test run to minimize possible errors. Figure 13 is a block diagram showing test instrumentation.

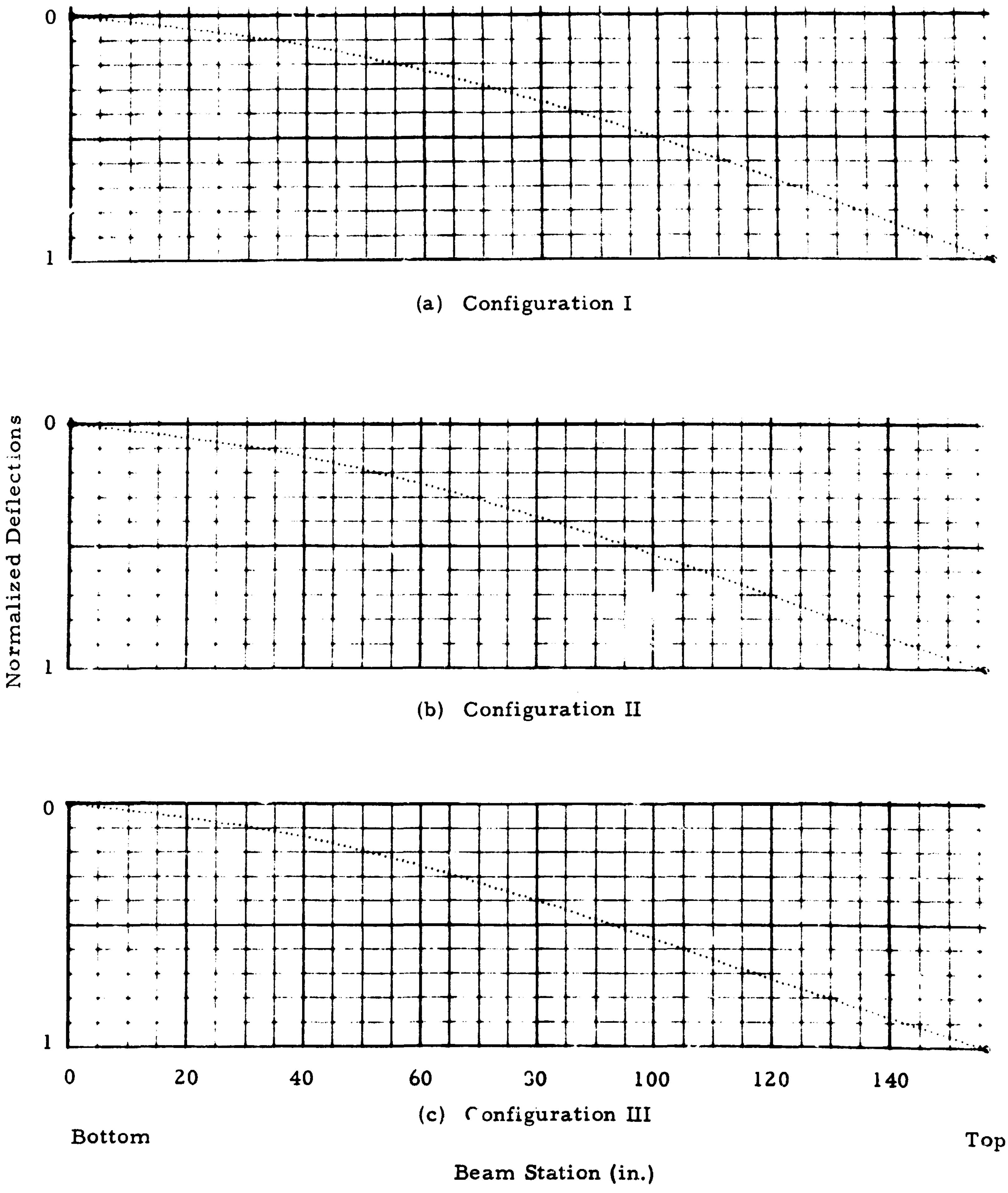

(a) Configuration I

(b) Configuration II

(c) Configuration III

Fig. 11 - Calculated Modal Deflection Shape

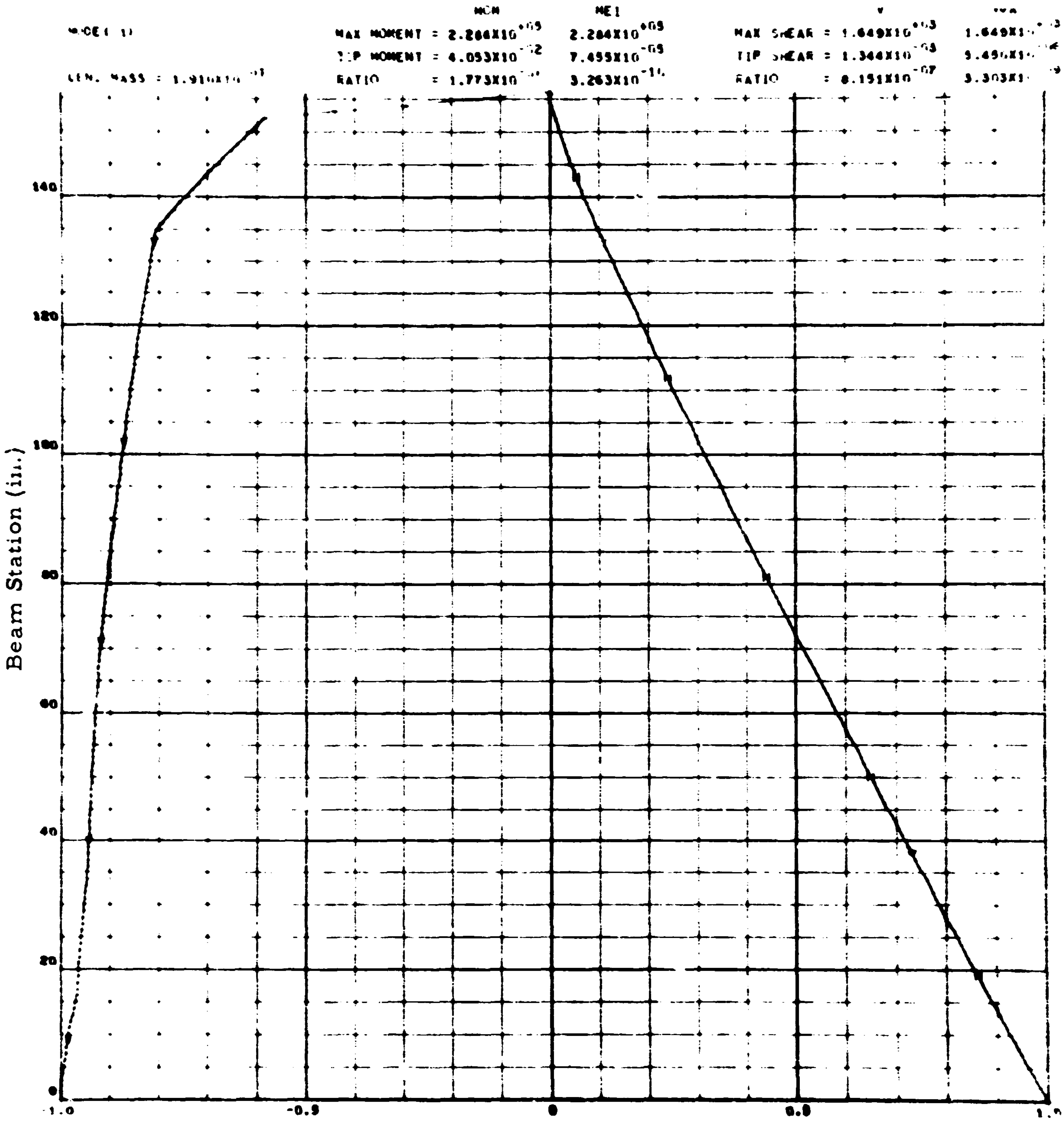

(d) Configuration I

Fig. 11 (Continued)

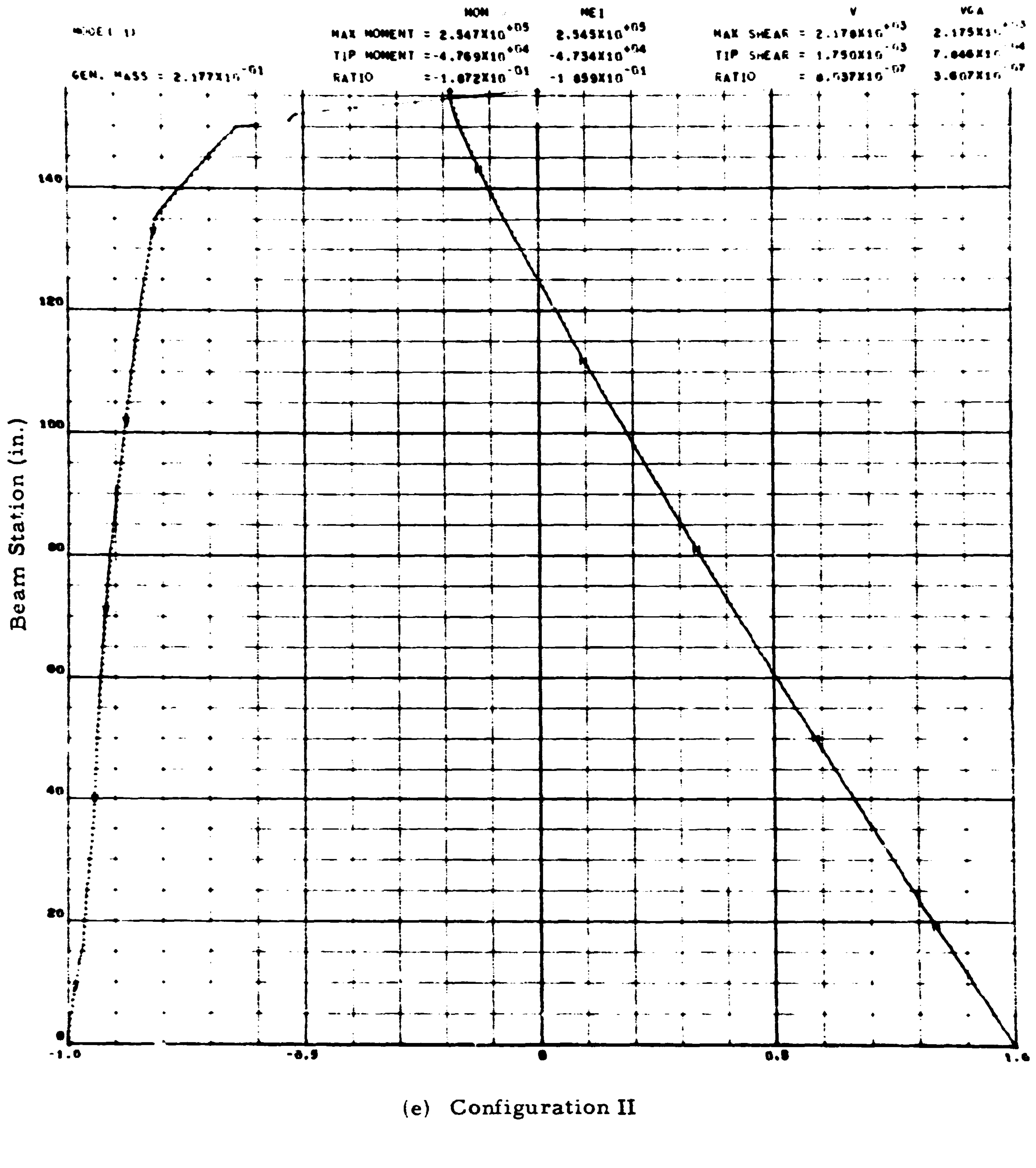

(e) Configuration II

Fig. 11 (Continued)

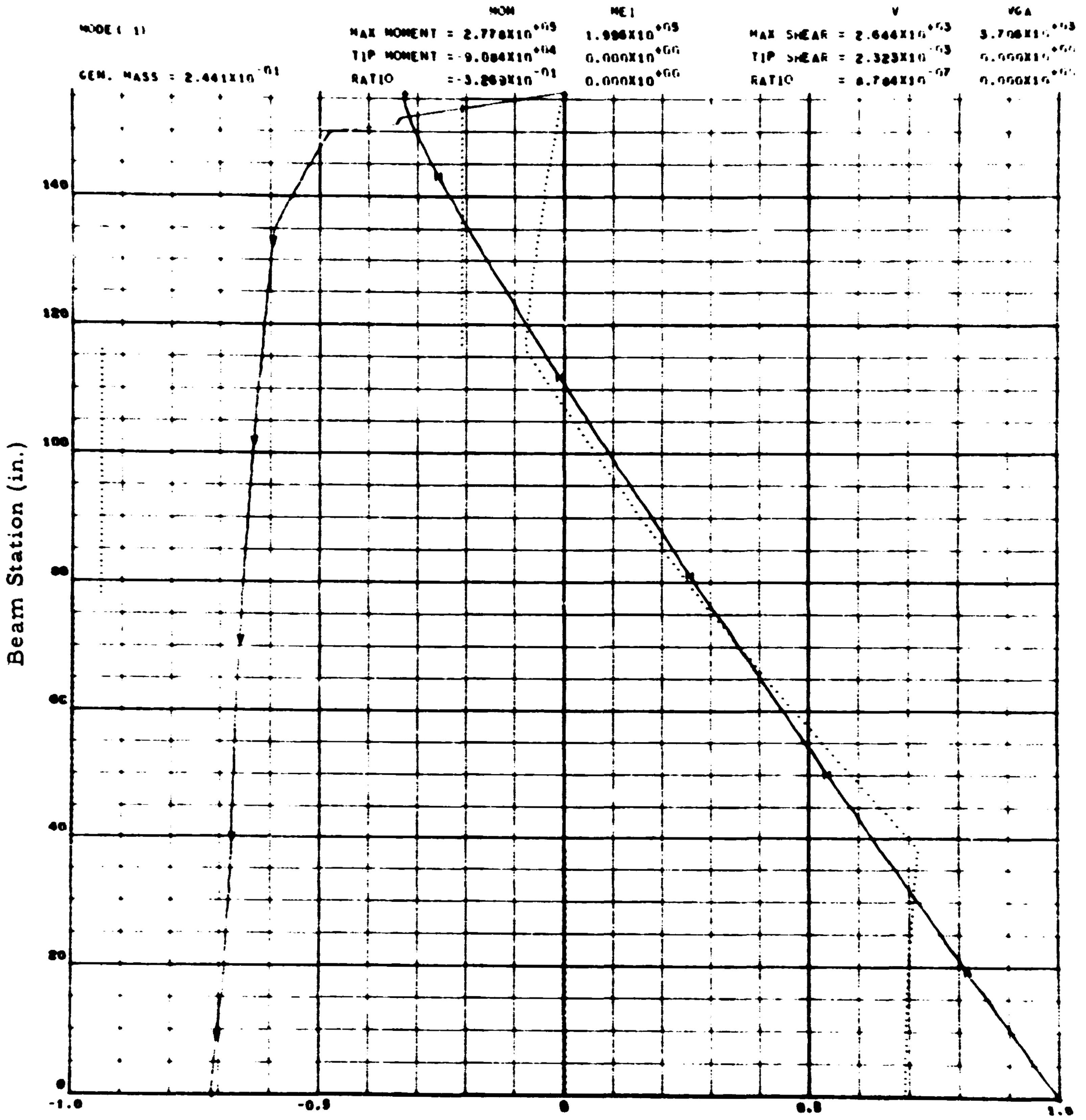

(f) Configuration III

Fig. 11 (Continued)

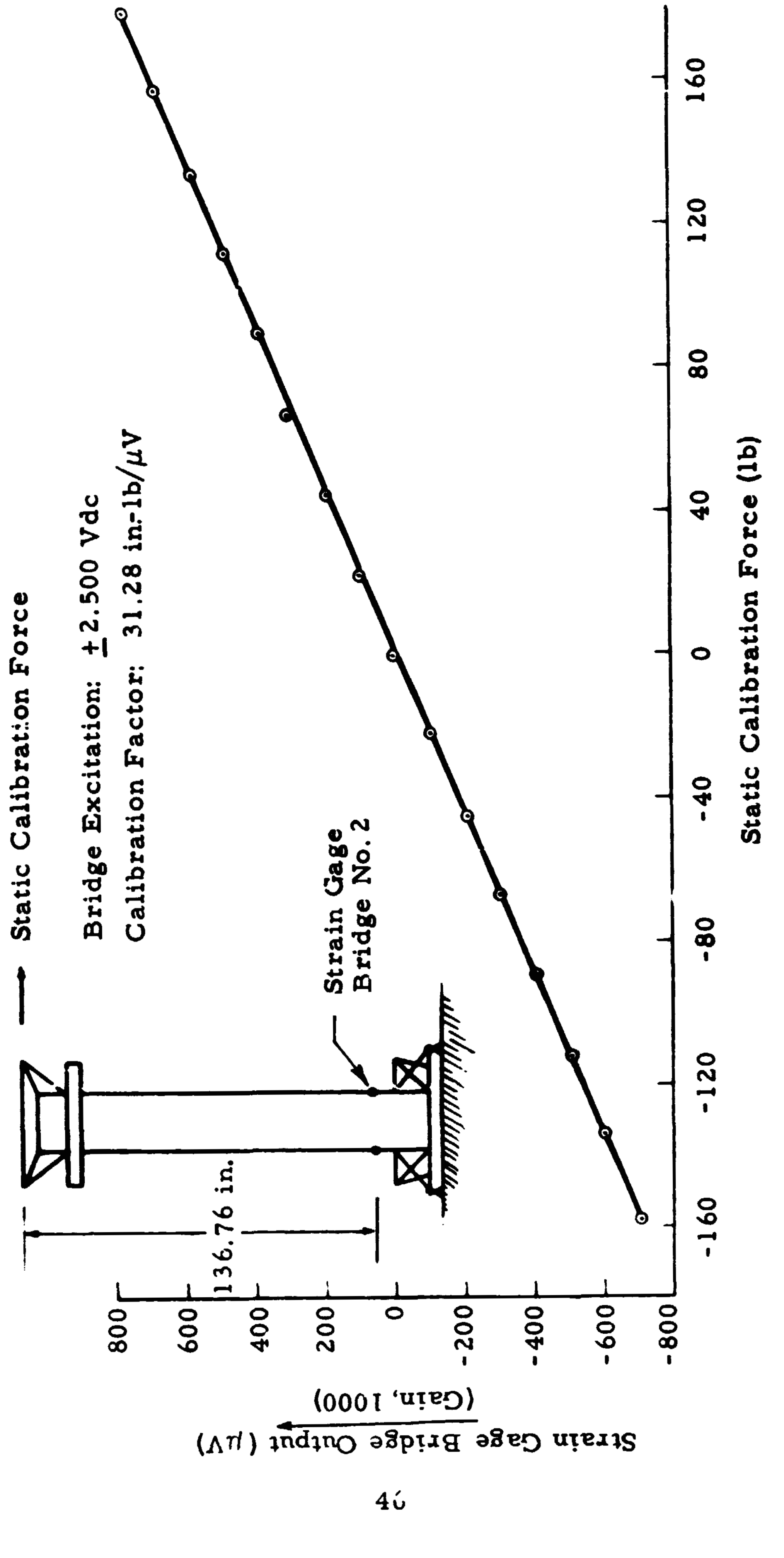

Fig. 12a - Strain Gage Bridge Calibration (Lower Bridge)

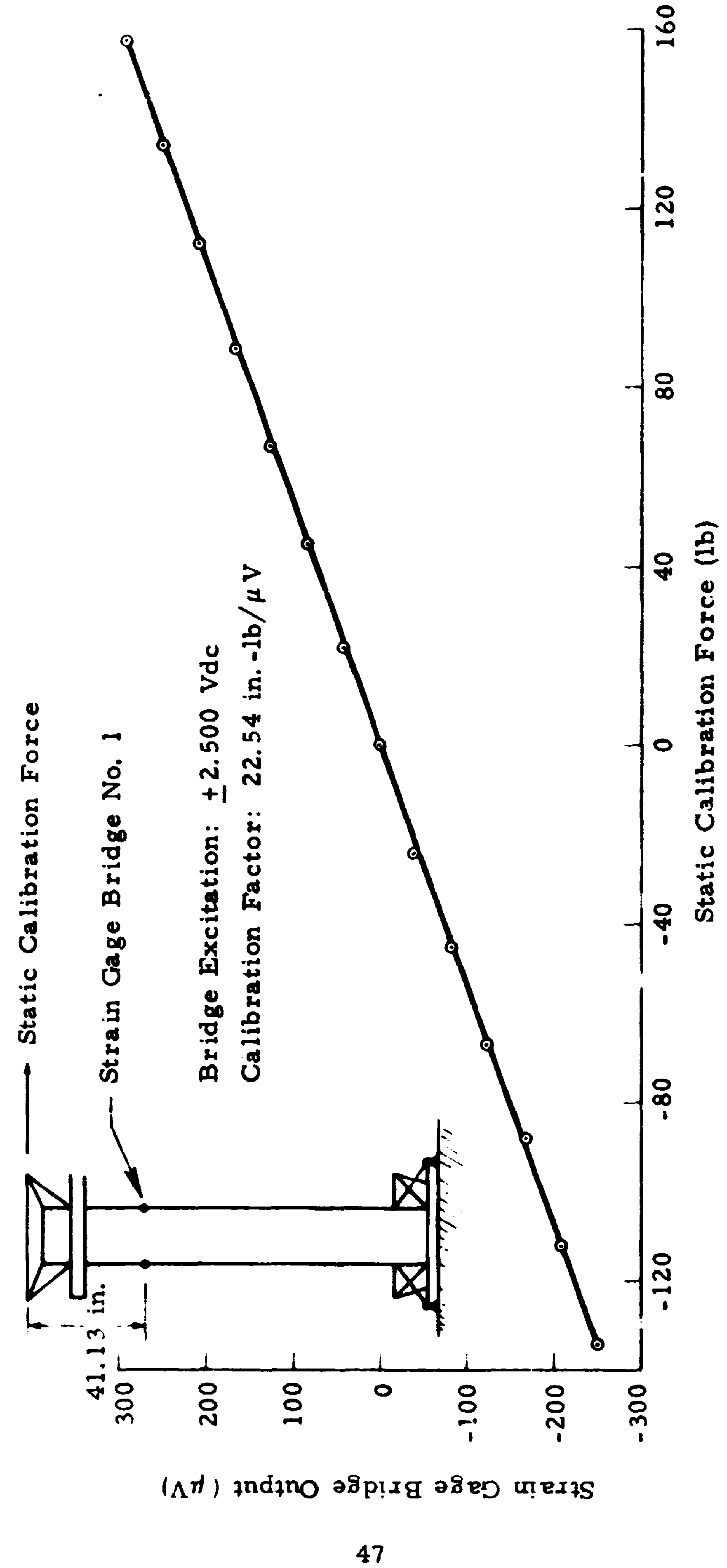

Fig. 12b - Strain Gage Bridge Calibration (Upper Bridge)

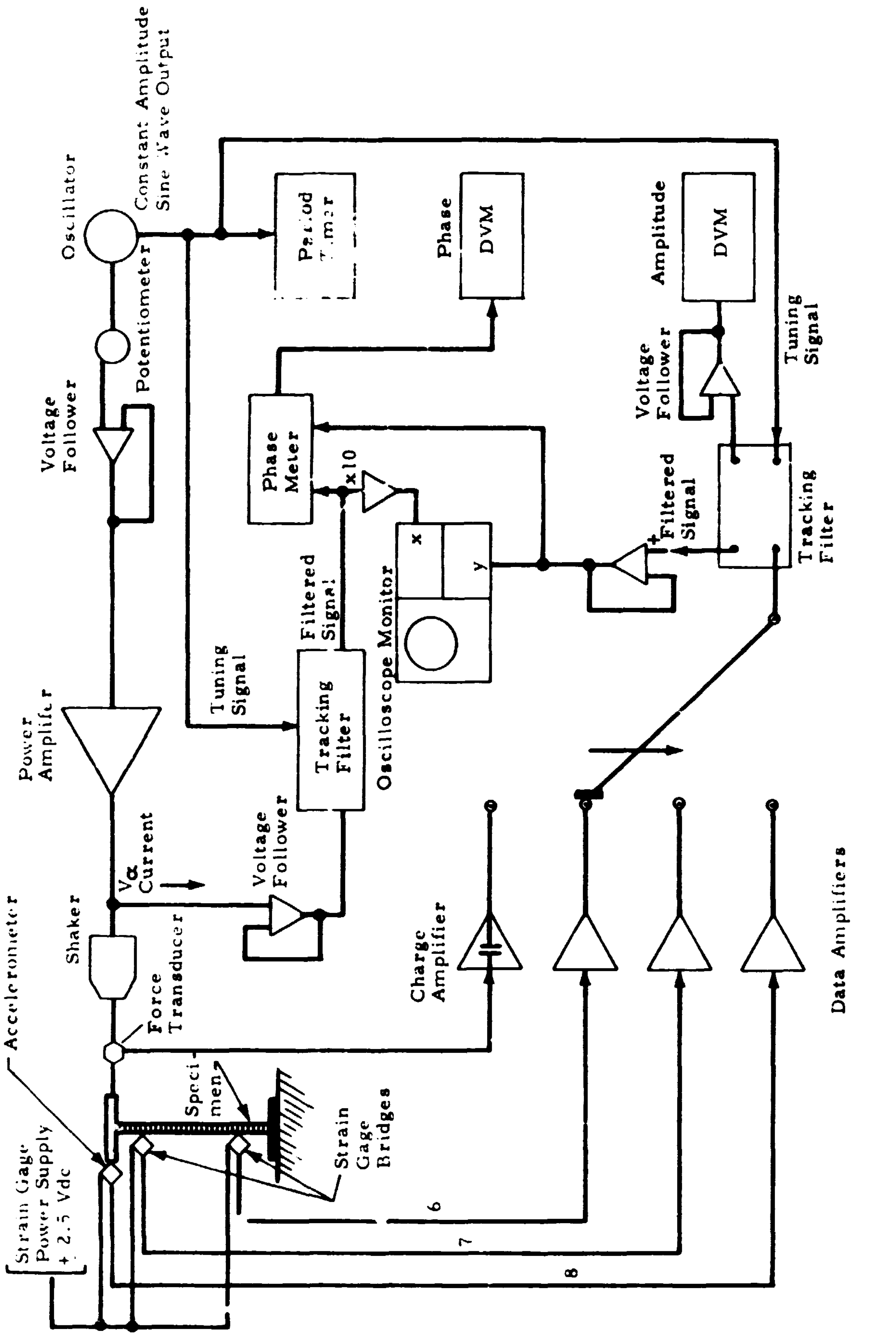

Fig. 13 - Test Instrumentation Block Diagram

4.4 TEST DESCRIPTION AND DATA

Several trial runs were made after the specimen was set up in Configuration I. Detailed modifications of procedures were introduced during and after these trial runs until a smooth operational procedure was achieved. Abnormal instrumentation behavior (drift, noise, jitter, etc.) was eliminated or minimized. Final test and data acquisition for all three configurations were made during one continuous twelve-hour run, stopping only for changing test specimen configuration.

For each configuration the 90-deg phase test was made first. The specimen was brought into resonance at the maximum excitation level and after steady-state had been reached. The following data were obtained:

Forcing Amplitude: F_1
Forcing Frequency: ω_1
Tip Acceleration — Fundamental Amplitude: $\omega_1^2 z_1$
Actual Phase Angle with Respect to Excitation

Bending Moments — Fundamental Amplitudes
Actual Phase Angles

The forcing amplitude F_1 was then decreased, and the above test and data were again obtained. This procedure was peated at evenly spaced forcing amplitudes in a decreasing order until transducer signals were so small that instrumentation noise prevented progressing further.

After testing at 90-deg phase differences between excitation and response, the entire procedure was repeated for tests at 45 deg, and at 135 deg.

After Configuration I tests were completed, the test specimen was modified for Configurations II and III tests. Identical test procedures were used for all configurations.

The first five columns in Tables 2a through 2c are data obtained from the above tests.

4.5 DATA ANALYSES

According to discussion in Section 3, the variation of the out-of-phase deflection was first investigated in order to determine whether the assumption of low nonproportional damping is justifiable. This was done by computing the ratio of measured bending moments to tip deflection, columns 7 and 8 in Tables 2a through 2c. Clearly, the dynamic deflection shape is independent of the frequency over the test frequency range. Nonproportional damping for all configurations is, therefore, low. The coefficients M and K in the modal equation may be regarded as constants with respect to frequency for each test configuration.

The first mode natural frequencies for each test configuration were obtained by plotting the relationship between 90-deg phase frequencies against tip displacement amplitudes from measurements and extrapolated to zero amplitude (Figs. 14a, 14b and 14c). The accuracy of extrapolation is judged to be approximately ± 0.2%. Frequency vs amplitude curves for 45-deg phase tests and for 135-deg phase tests are also included in the figures. The function $f_s(z)/M$ for each test configuration was determined from the 90-deg test accorind to Eq. (61) by plotting the quantity $\left[\bar{\omega}_1{}^2 - \omega_1{}^2(z_1)\right] z_1$ against z_1 (see Figs. 15a, b, and c).

For all three configurations, the empirial relationship

$$\frac{1}{M} f_s(z_1) = - \left[\bar{\omega}_1{}^2 - \omega_1{}^2(z_1)\right] z_1 = A z_1{}^{1.5} \tag{68}$$

appears to hold. The ratio

$$A = \frac{\left[\bar{\omega}_1{}^2 - \omega_1{}^2 (z_1)\right] z_1}{z_1{}^{1.5}}$$

Table 2a

CONFIGURATION I DATA

$\bar{\omega}_1$ = 87.4 (rad/sec) ± .2%

A = 1,064 $(sec^{-2}\text{-}in^{-0.5})\ ^{+2.5\%}_{-2.0\%}$

B = 86.07 $(lb/in^{-1.5})\ ^{+6\%}_{-4\%}$

M = 0.1864 $(lb\text{-}sec^2/in.)\ ^{+2.3\%}_{-1.8\%}$

M_2 = 1.86 x 10^5 (in-lb/in.) ± 1.0%

M_1 = 0.259 x 10^5 (in-lb/in.) ± 0.6%

Col. No. Symbol	(1) ω	(2) $\omega^2 z$	(3) F	(4) M_2	(5) M_1	(6) z	(7) M_2/z	(8) M_1/z	(9) A	(10) M	(11) B
Def.	Freq.	Tip Accel.	Applied Force	Bending Moment	Bending Moment	Tip Deflection				Generalized Mass	
Units	rad/sec	in/sec^2	lb	in-lb	in-lb	in.	10^5 lb	10^5 lb		$lb\text{-}sec^2/in.$	lb
90-deg Test	85.184	981.6	4.5280	25,040	3,383.0	.13530	1.85	.2500	1,039		90.89
	85.396	779.5	3.1300	19,990	2,750.0	.10690	1.87	.2660	1,059		89.56
	85.592	635.9	2.1790	16,360	2,247.0	.08678	1.89	.2590	1,062		85.25
	85.801	492.8	1.4260	12,620	1,743.0	.06694	1.89	.2604	1,071		87.33
	85.986	373.6	0.9559	9,584	1,322.0	.05053	1.90	.2616	1,091		84.15
	86.260	249.1	0.5162	6,190	871.6	.03348	1.85	.2603	1,082		84.26
	86.623	125.4	0.2383	3,128	442.5	.01671	1.87	.2648	1,046		110.40
135-deg Test	86.520	1,015.0	8.0830	25,020	3,449.0	.13560	1.85	.2540		.1832	
	86.687	745.5	5.3770	18,390	2,525.0	.09920	1.86	.2550		.1844	
	86.963	493.4	3.4760	12,200	1,703.0	.06524	1.87	.2610		.1909	
	87.466	228.0	1.6010	5,617	771.2	.02980	1.88	.2590		.1907	
	87.941	112.5	0.8296	2,714	375.7	.01455	1.87	.2580		.1831	
45-deg Test				25,070	3,493.0	.13830	1.81	.2530			
				19,710	2,742.0	.10870	1.81	.2530			
				13,760	1,933.0	.07471	1.84	.2590			
				6,910	976.7	.03729	1.85	.2620			
				2,825	394.0	.01496	1.90	.2630			

Table 2b

CONFIGURATION II DATA

$\bar{\omega}_1$ = 93.1 (rad/sec) ± 0.2%

A = 1,111 (sec^{-2}-$in^{-0.5}$) $^{+2\%}_{-5\%}$

M = .2183 $^{+2.4\%}_{-3.6\%}$

M_2 = 1.726 x 10^5 (in-lb/in.)

M_1 = 0.423 x 10^5 (in-lb/in.)

Col. No.	(1)	(2)	(3)	(4)	(5)	(6)	(7)	(8)	(9)	(10)	(11)	(12)
Symbol	ω	$\omega^2 z$	F	M_2	M_1	z	M_2/z	M_1/z	A	M	Spider-beam	(11)÷(6)
Def.	Freq.	Tip Accel.	Force	Bending Moment	Bending Moment	Tip Deflection				Generalized Mass	Damping Force	
Units	rad/sec	in/sec^2	lb	in.-lb	in.-lb	in.	10^5 lb	10^5 lb		lb-sec^2/in.	lb	
90-deg Test	90.406	1,782.0	9.502	36,770	9,016	.21800	1.69	.414	1,059		1.460	6.69
	90.667	1,347.0	6.371	27,870	6,850	.16380	1.70	.418	1,105		1.130	6.90
	90.874	1,121.0	4.872	23,330	5,700	.13570	1.72	.420	1,112		0.970	7.15
	91.086	887.7	3.539	18,580	4,561	.10700	1.74	.426	1,134		0.772	7.21
	91.389	648.8	2.272	13,480	3,328	.07768	1.74	.428	1,133		0.560	7.21
	91.681	454.3	1.366	9,405	2,306	.05405	1.74	.426	1,128		0.372	6.88
	91.947	313.2	0.823	6,495	1,578	.03705	1.75	.426	1,108		0.259	6.99
135-deg Test	91.973	1,814.0	17.330	36,270	9,106	.21440	1.69	.425		.2100		
	92.141	1,365.0	12.320	27,430	6,740	.16080	1.71	.419		.2085		
	92.301	1,106.0	9.853	22,300	5,477	.12990	1.72	.422		.2182		
	92.483	880.1	7.870	17,760	4,357	.10290	1.73	.423		.2226		
	92.720	683.4	6.286	13,830	3,401	.97949	1.74	.428		.2234		
	93.043	441.8	3.952	8,821	2,929	.05103	1.73	.479		.2223		
	93.472	221.8	2.002	4,473	1,089	.02539	1.76	.429		.2237		
45-deg Test				37,010	9,081	.21860	1.69	.415				
				27,710	6,762	.16270	1.70	.416				
				23,240	5,649	.13500	1.72	.418				
				17,450	4,274	.10090	1.73	.424				
				12,980	3,162	.07466	1.74	.424				
				9,506	2,313	.05418	1.75	.427				
				4,504	1,088	.02553	1.76	.426				

Table 2c

CONFIGURATION III DATA

$\bar{\omega}$ = 95.3 (rad/sec) $\pm$ 0.2%

A = 1,229 $(sec^{-2}\text{-}in^{-0.5})\ ^{+\ 5.5\%}_{-\ 2.5\%}$

M = .2513 $(lbs\text{-}sec^2/in.)\ ^{+\ 2.4\%}_{-\ 4.1\%}$

M_2 = 1.71 x 10^5 (in-lbs/in.)

M_1 = .959 x 10^5 (in-lbs/in.)

Col. No.	(1)	(2)	(3)	(4)	(5)	(6)	(7)	(8)	(9)	(10)	(11)	(12)
Symbol	ω	$\omega^2 z$	F	M_2	M_1	z	M_2/z	M_1/z	A	M	Spider-beam	(11)÷(6)
Def.	Freq.	Tip Accel.	Force	Bending Moment	Bending Moment	Tip Deflection				Generalized Mass	Damping Force	
Units	rad/sec	in/sec^2	lb	in-lb	in-lb	in.	lb	lb		lb-sec^2/in.	lb	
90-deg Test	92.871	1,256.0	6.9720	24,370	13,546	.14560	1.6740	.9310	1,198		2.1180	15.03
	93.062	1,043.0	5.0190	20,330	11,340	.12040	1.6890	.9420	1,215		1.7450	14.49
	93.195	845.9	3.7970	16,490	9,205	.09740	1.6930	.9450	1,272		1.4140	14.52
	93.497	629.3	2.5640	12,290	6,852	.07199	1.7070	.9520	1,269		1.0500	14.59
	93.653	516.6	2.0000	10,090	5,613	.05890	1.7130	.9530	1,282		0.8800	14.94
	93.875	407.1	1.4220	8,112	4,438	.04620	1.7560	.9610	1,263		0.6940	15.02
	94.266	280.5	.9093	5,451	2,948	.03157	1.7270	.9340	1,103		0.4697	14.88
	94.748	114.6	.2981	2,237	1,240	.01277	1.7520					
							1.7138	.9450				
135-deg Test	94.461	1,299.0	15.245	24,090	13,524	.14560	1.6500	.9290		.2411		
	94.545	1,071.0	12.260	20,110	11,220	.11980	1.6800	.9370		.2560		
	94.764	844.3	9.682	15,780	8,836	.09402	1.6800	.9400		.2558		
	94.987	623.9	6.907	11,730	6,537	.06915	1.7000	.9450		.2554		
	95.135	505.9	5.709	9,609	5,353	.05590	1.7300	.9580		.2575		
	95.305	428.5	4.801	8,059	4,501	.04718	1.7100	.9540		.2541		
	95.545	309.2	3.380	5,842	3,245	.03387	1.7200	.9580		.2492		
	95.661	218.6	2.087	4,149	2,306	.02389	1.7400	.9650		.2418		
							1.7010	.9482				
45-deg Test				24,260	13,530	.14480	1.6800	.9340				
				20,670	11,580	.12310	1.6800	.9410				
				15,649	8,723	.09228	1.7000	.9450				
				11,900	6,694	.06991	1.7000	.9560				
				10,230	5,774	.05967	1.7100	.9680				
				8,352	4,756	.04975	1.6800	.9560				
				5,839	3,275	.03384	1.7300	.9680				
				3,986	2,224	.02298	1.7300	.9680				

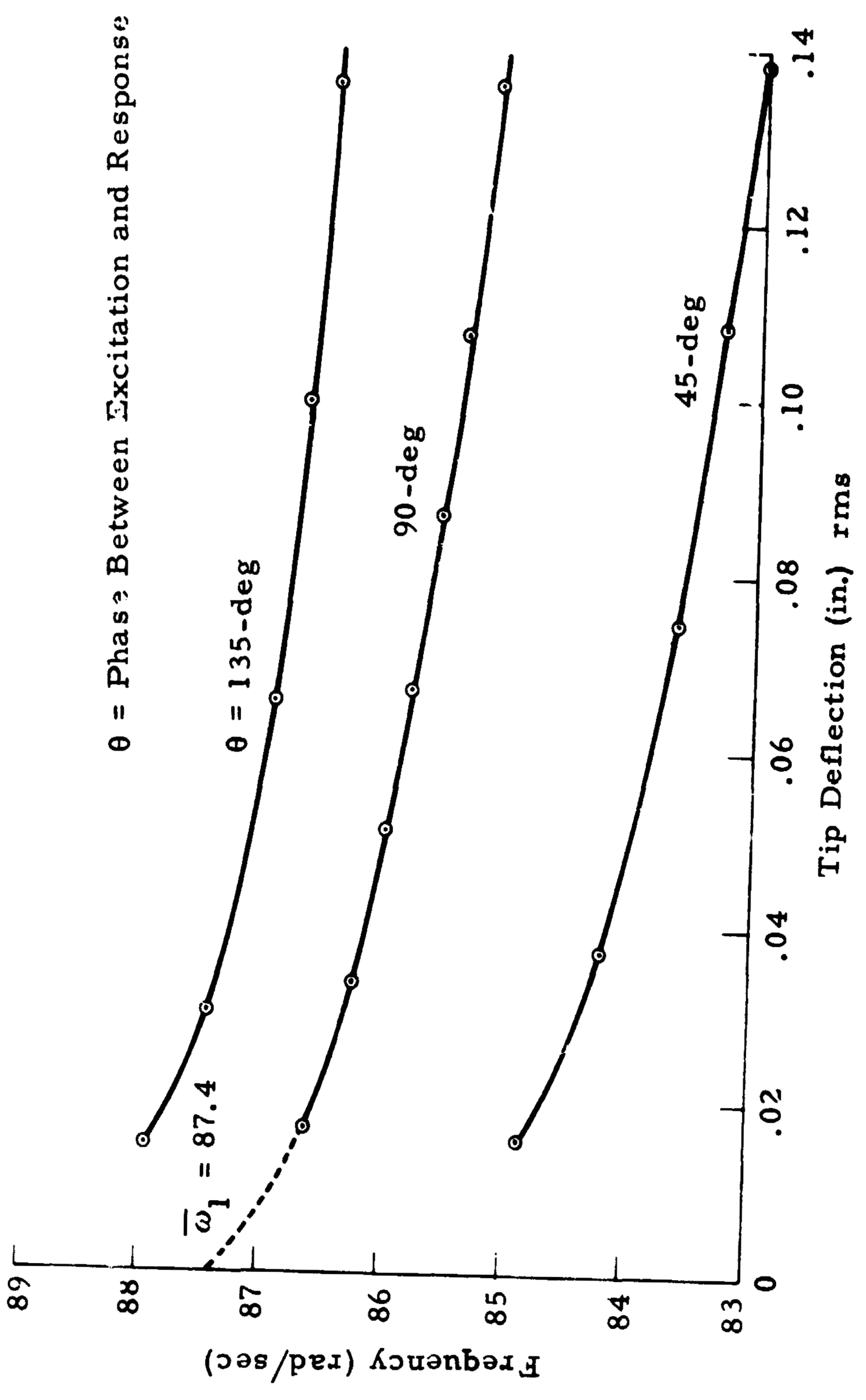

Fig. 14a - Variation of Resonant Band Frequencies with Response Amplitude (Configuration I)

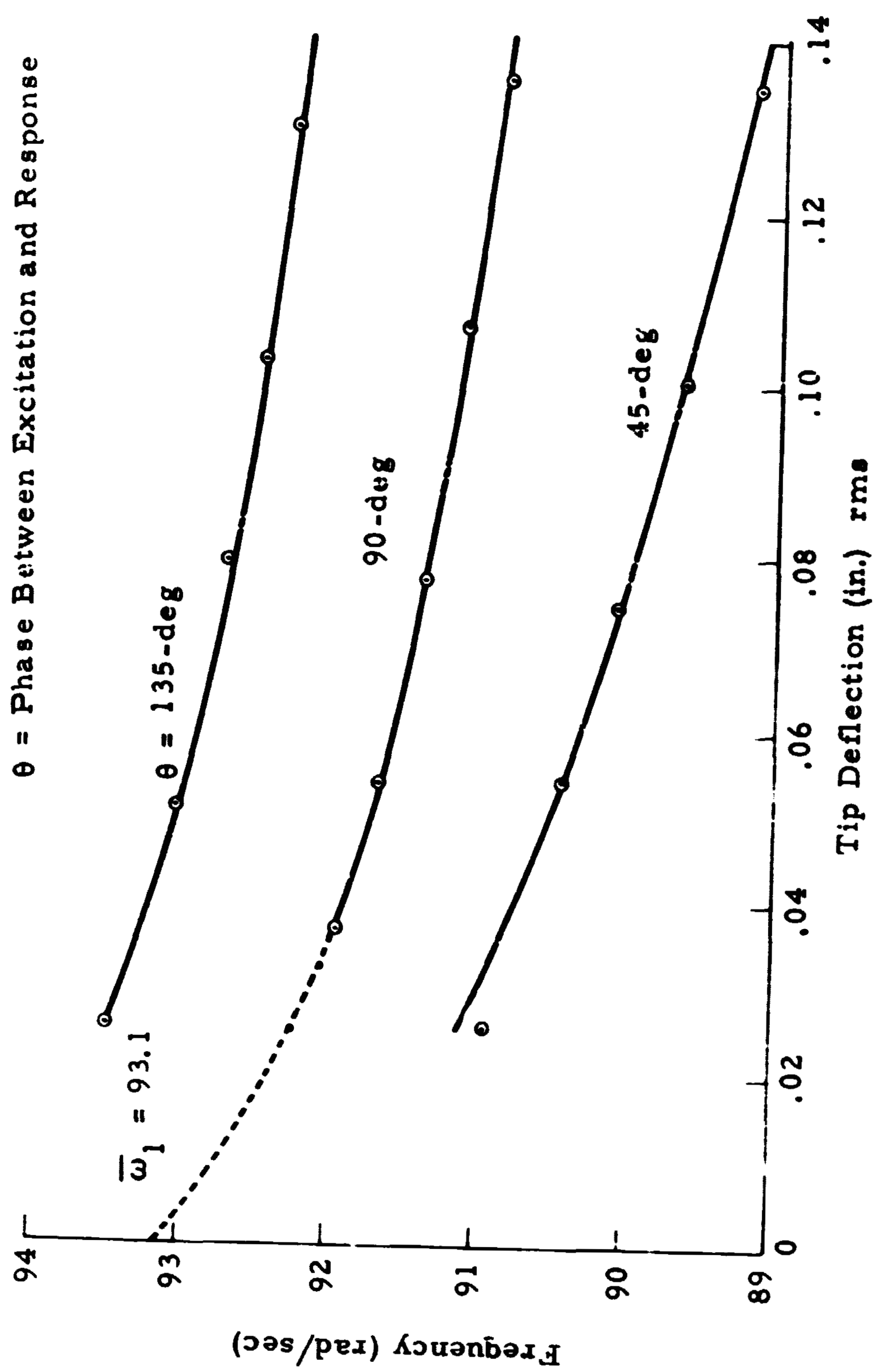

Fig. 14b - Variation of Resonant Band Frequencies with Response Amplitude (Configuration II)

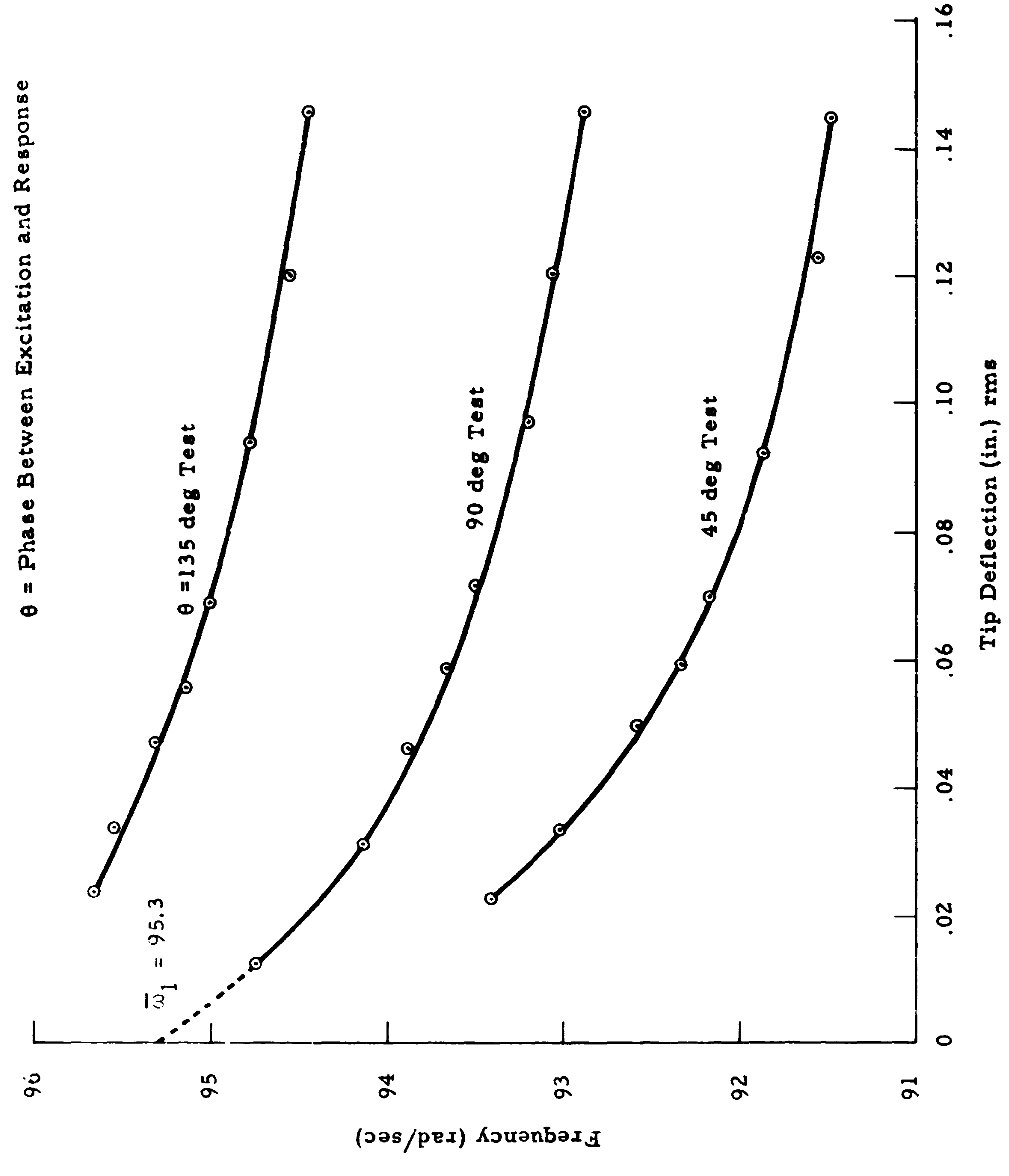

Fig. 14c - Variation of Resonant Band Frequencies with Response Amplitude (Configuration III)

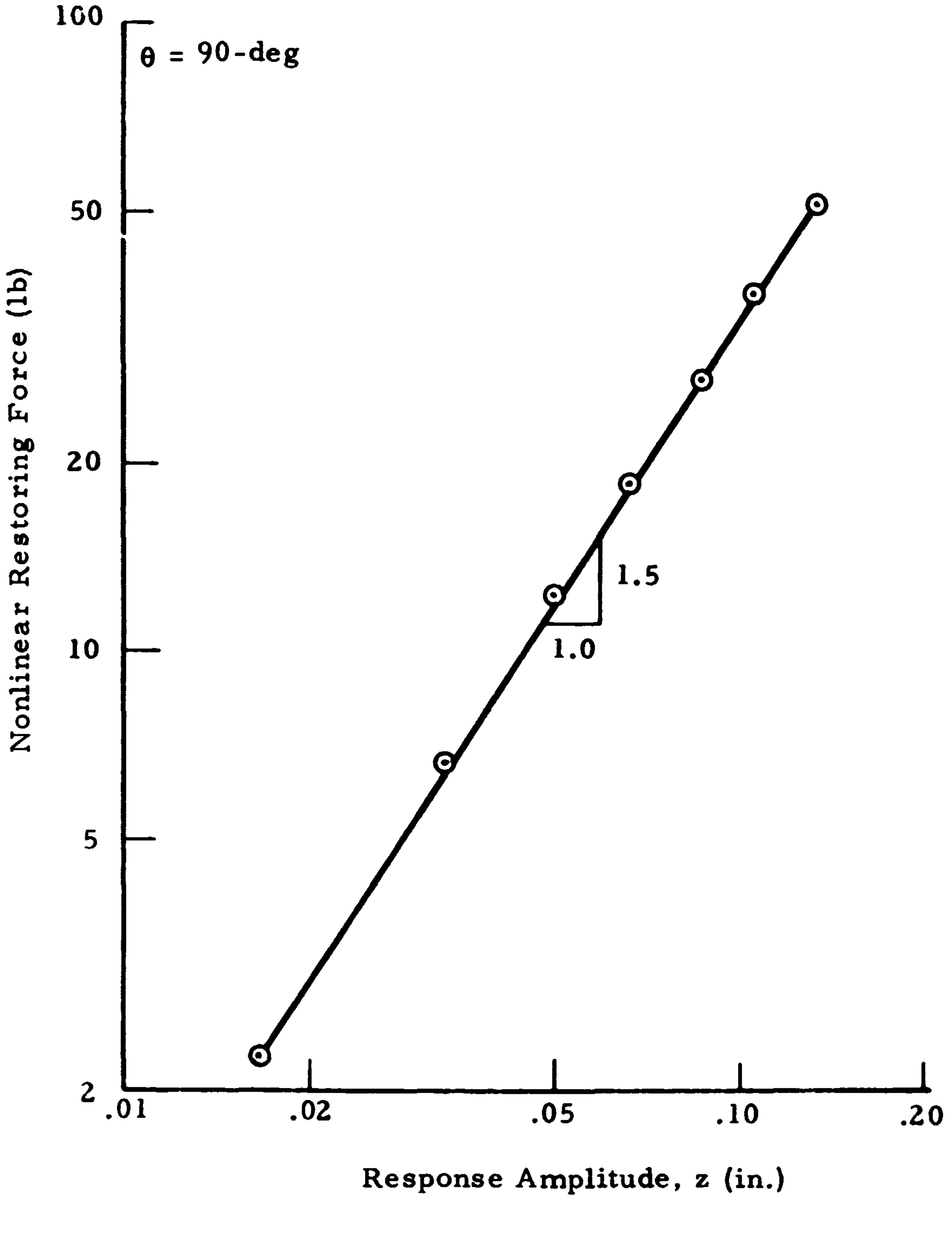

Fig. 15a - Nonlinear Restoring Force (Configuration I)

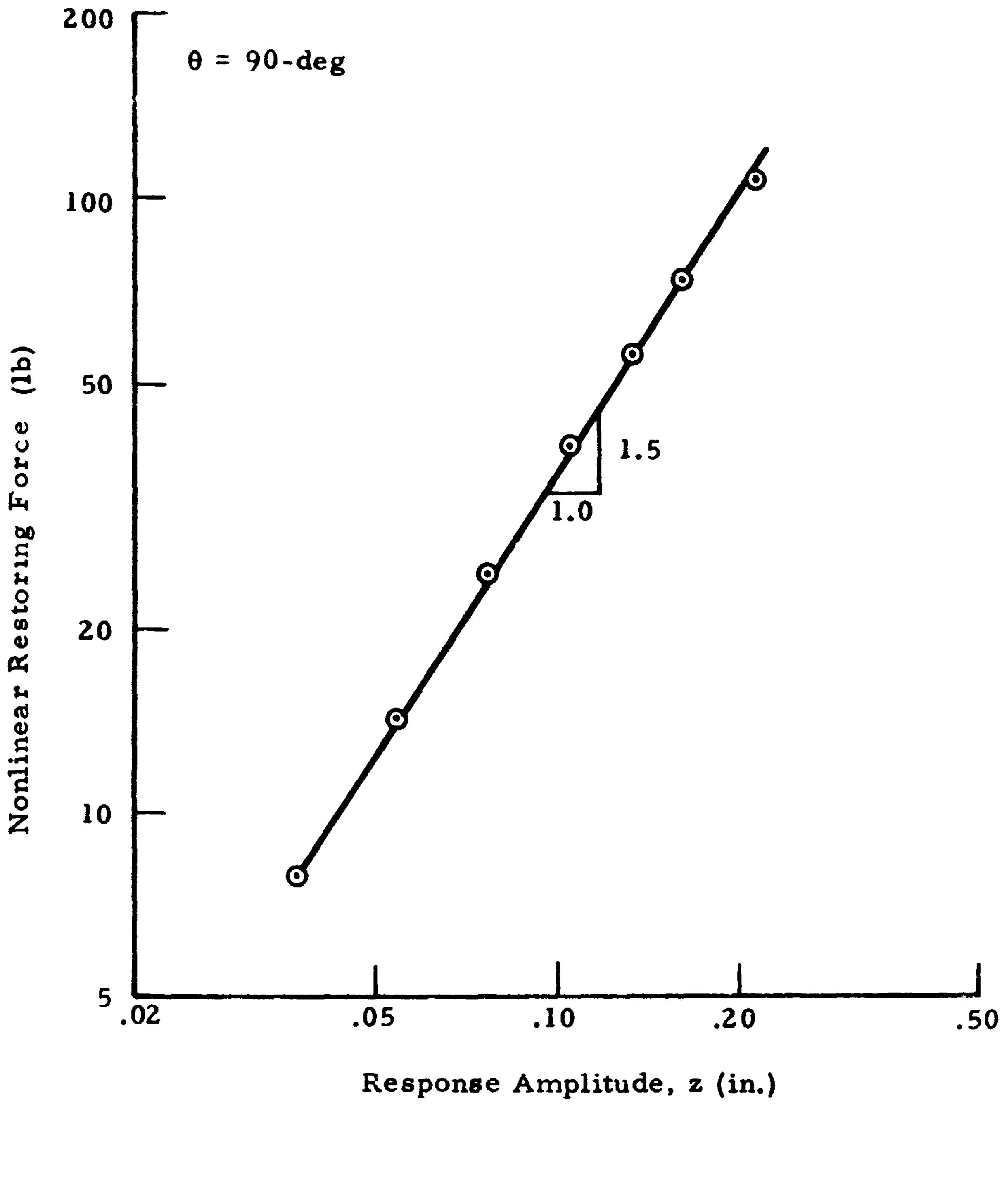

Fig. 15b - Nonlinear Restoring Force (Configuration II)

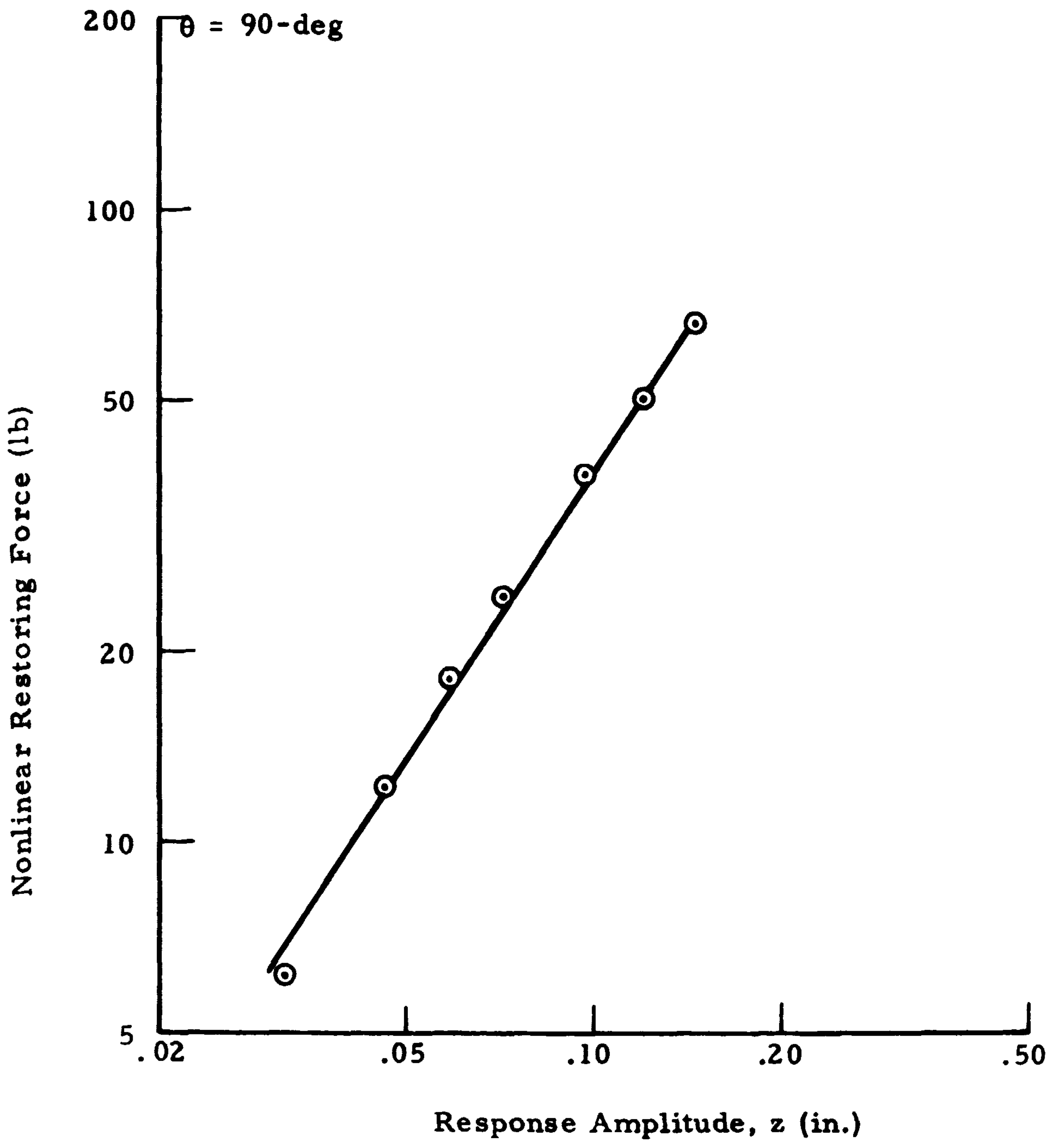

Fig. 15c - Nonlinear Restoring Force (Configuration III) was computed for each configuration at each test amplitude z_1 (column 9 in Tables 2a, b, and c). It is seen that

$$A = 1064\ (\text{sec}^{-2}\ \text{in}^{-0.5})\ {}^{+2.5\%}_{-2.0\%} \quad \text{for Configuration I}$$

$$A = 1111\ (\text{sec}^{-2}\ \text{in}^{-0.5})\ {}^{+2.0\%}_{-5.0\%} \quad \text{for Configuration II}$$

$$A = 1229\ (\text{sec}^{-2}\ \text{in}^{-0.5})\ {}^{+5.5\%}_{-2.5\%} \quad \text{for Configuration III}$$

The constant M for each configuration was computed from the above values of A and data for the 135-deg phase tests. Equation (66) was used with θ = 135-deg. The results are (Column 10, Tables 2a, b, and c).

$$M = .1864\ (\text{lb-sec}^2/\text{in})\ {}^{+2.3\%}_{-1.8\%} \quad \text{for Configuration I}$$

$$M = .2183\ (\text{lb-sec}^2/\text{in})\ {}^{+2.4\%}_{-3.6\%} \quad \text{for Configuration II}$$

$$M = .2432\ (\text{lb-sec}^2/\text{in})\ {}^{+5.9\%}_{-6.9\%} \quad \text{for Configuration III}$$

These average values compare favorably with analytical results of the undamped structure listed in Table 1 (differences of -2.5%, 0%, +0.8%, respectively).

Because the out-of-phase deflection shapes do not vary with frequency, nonproportional damping must be low for all three configurations studied. Damping properties may be determined either as proportionally distributed damping or as concentrated damping lumped at the ends. Both methods of description are equally suitable.

Material damping and air damping for test Configuration I are estimated in Appendix A. Calculated mode shape for the undamped specimen is used. Results indicate that their contribution to the total damping is extremely small and negligible.

Damping of the specimen in Configuration I is determined in terms of an amplitude-dependent modal damping coefficient. In Configurations II and III the total damping is described as the sum of two parts, the (already determined) damping of Configuration I, plus concentrated damping due to dissipations occurring in the spider beam structure which undergoes cyclic strain in vibrations of Configurations II and III.

Equation (67) in Section 3.4 indicates that the out-of-phase amplitude of the function $f(\dot{Z}, \dot{Z})$ in Eq. (47) in a steady-state test is given by the applied forcing amplitude when the phase angle is 90 deg:

$$f_c(z_1) = F_1(z_1) \tag{69}$$

For Configuration I, $F_1(z_1)$ was plotted in Fig. 16a. It was found that

$$f_c(z_1) = F_1(z) = B\, z^{1.5} \tag{70}$$

The value of B was computed for each test point and, as shown in Column 11, Table 2a,

$$B = 86.07 \quad \text{lb/(in.)}^{1.5}$$

on the average. The range of data scatter is +6% to -4%. Therefore, the nonlinear function $f(Z, \dot{Z})$ has the following properties:

$$f(Z, 0) = 0$$

i.e., the structure is statically linear as the strain gage calibration has indicated,

$$f_s = \frac{1}{\pi} \int_0^{2\pi/\omega} f(Z, \dot{Z}) \sin(\omega t - \theta)\, dt = -AM\ z^{1.5}$$

and

$$f_c = \frac{1}{\pi} \int_0^{2\pi/\omega} f(Z, \dot{Z}) \cos(\omega t - \theta)\, dt = B\ z^{1.5}$$

with $-AM = 198.3\ \mathrm{lb/(in.)}^{1.5}$

$B \quad = 86.07\ \mathrm{lb/(in.)}^{1.5}$

In Ref. 3, nonlinear hysteresis damping was considered by assuming perfect elastic-plastic properties of structural elements, according to suggestions in Refs. 5 and 6. The resulting damping law is truely rate independent, i.e., the structure would be nonlinear statically if it is nonlinear dynamically. Furthermore, if

$$f_s = -A'M\ z^n$$

and

$$f_c = B'\ z^n$$

then, it is necessary that

$$A'M = \frac{n}{4(n-2)}\ \pi B' \tag{71}$$

Equation (71) is not satisfied by the experimental results of the current study where n = 2.5. Modifications of the fundamental hysteresis damping is, therefore required. These modifications are:

1. The recognization that hysteresis damping is not entirely frequency independent, and that the damping law cannot be extended to include static deformation processes. For a wide range of non-zero frequencies, however, damping may still be made constant with respect to frequency so that it is still possible to synthesize damping of a given structure in terms of nonlinear hysteresis damping properties in the manner shown in Ref. 3.

2. A nonlinear, conservative restoring force

$$
\begin{aligned}
f_r(Z, \dot{Z}) \quad &\propto \quad Z\left|Z\right|^{1.5}, \quad \left|\dot{Z}\right| > \epsilon \\
&= \quad 0 \qquad\qquad\quad \left|\dot{Z}\right| < \epsilon
\end{aligned}
\tag{72}
$$

is to be included. Then

$$
f_s(z) = \frac{1}{\pi} \int_0^{2\pi/\omega} f_r \sin(\omega t - \theta)\, dt - \frac{n\pi}{4(n-2)} B\ z^{1.5} \tag{73}
$$

and Eq. (71) may be satisfied.

The damping in Configuration I is then synthesized as a dynamic hysteresis damping for which, according to Ref. 3, the energy dissipation per cycle of vibration is

$$
D = J\ z^{2.5} \tag{74}
$$

The locus of the tips of hysteresis loops is given by

$$
F(z) = Kz - \frac{n\pi}{4(n-2)} B\ z^{n-1} \tag{75}
$$

with

$$
n = 2.5, \quad B = 86.07
$$

The damping of the spider-beam structure is determined by tests with the specimen in Configurations II and III. Damping of the center structure was isolated and separated by subtracting from the damping force the quantity

$$z^{1.5}(86.07)\,(m_2/z)_I^{1.5}/(m_2/z)_{II}^{1.5}$$

or

$$z^{1.5}(86.07)\,(m_2/z)_I^{1.5}/(m_2/z)_{III}^{1.5}$$

as the case may be. The quantity $(m_2/z)_I^{1.5}$ is the bending moment per unit tip deflection in Configuration I, etc.

The remaining damping forces were plotted against the tip response amplitude (Fig. 16b) and linear relationships are observed for both Configurations II and III. The constants of proportionality are computed, columns 12, Tables 2b and 2c), and have average values of 7.00 lbs/in. tip deflection for Configuration II and 14.78 lb/in. tip deflection for Configuration III.

The above damping properties are associated with spider beam deformations and may be expressed as a hysteresis damping force at the spider-beam associated with linear deflection at the point of outer LOX tank attachment point with respect to the center LOX tank attachment point.

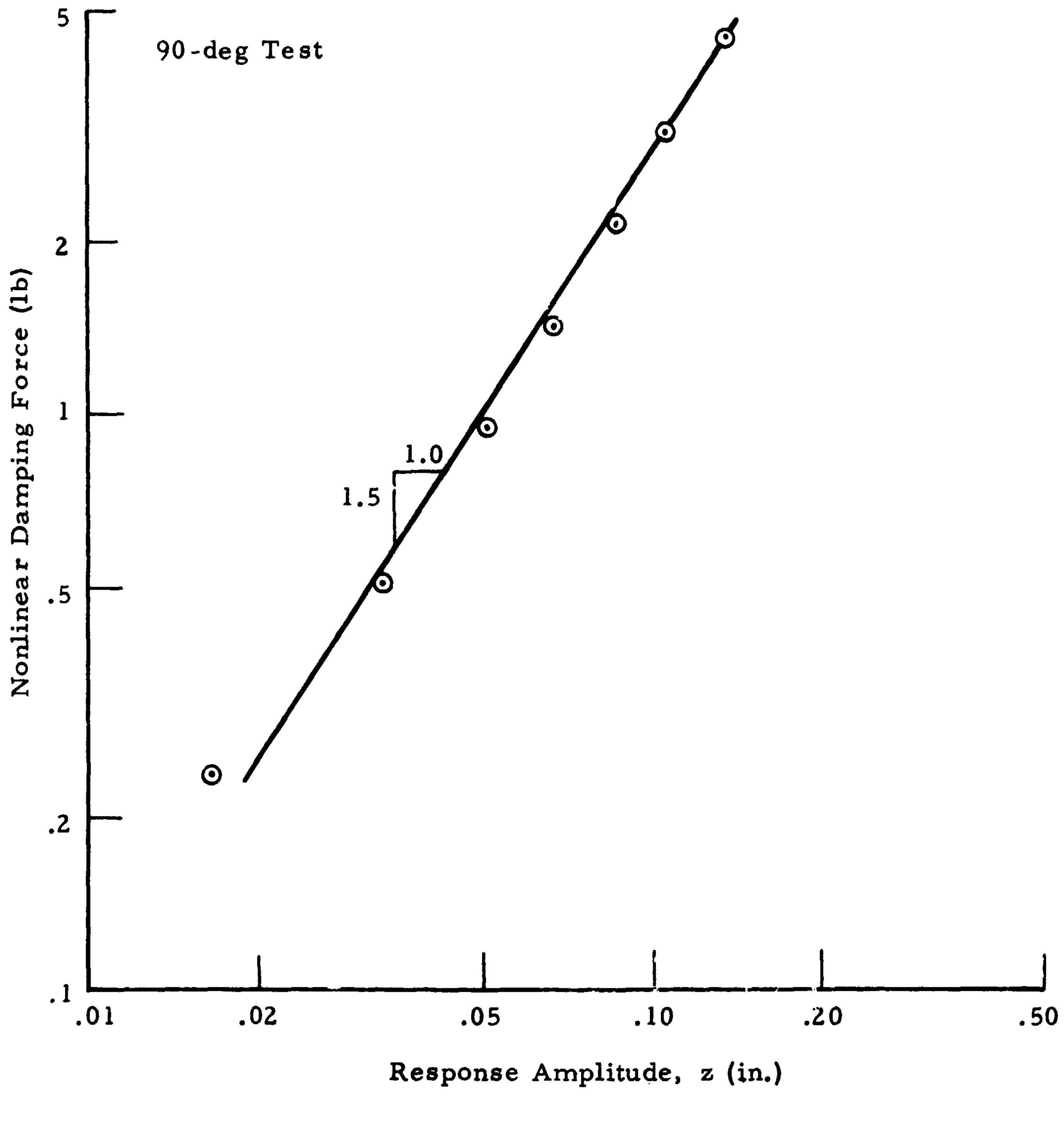

Fig. 16a - Nonlinear Damping Force (Configuration I)

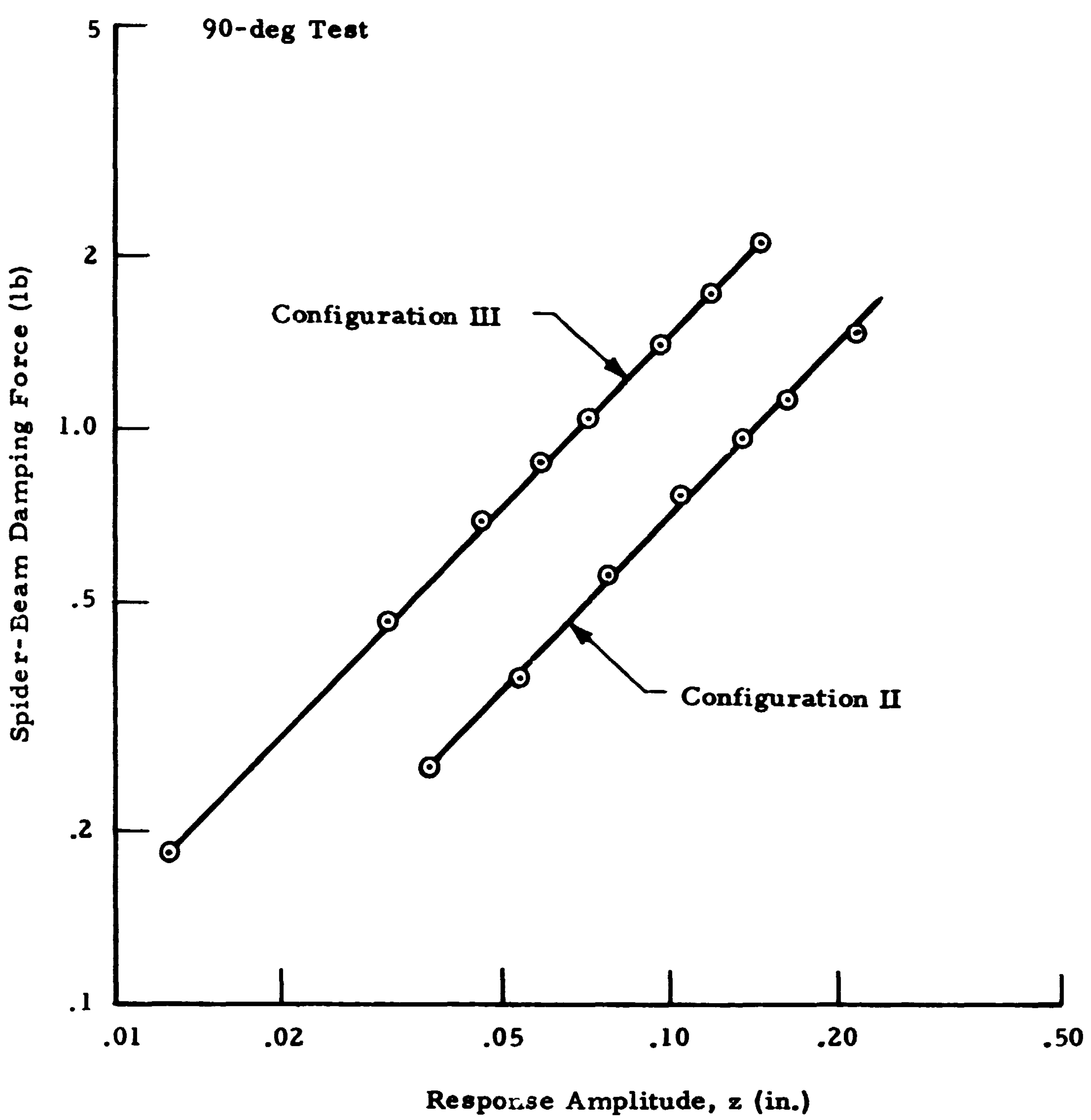

Fig. 16b - Damping Force Due to Spider-Beam Deformation

Section 5
CONCLUSIONS AND RECOMMENDATIONS

The analysis of a simple beam with a dissipative end condition led to simple solutions that are easily related to physical properties of the structure. The method of analysis appears to be equally applicable for other structural components, as well as for substructures of greater complexity than rods, beams, plates, etc. Based on such considerations, definition of modal responses and modal coefficients such as generalized mass, damping coefficients, etc., (which can be related to physical properties of structures) are proposed for the case of nonproportional damping. If nonproportionality is small, modal coefficients can be assumed to be constant even if total damping is not low.

The experimental demonstration of the test approach of physically substructuring complicated structures and testing them and joints individually was successful for the specimen employed. This success inevitably leads to the postulation that substructure testing and analyses may eventually replace expensive tests of totally assembled complex structures. Advantages of substructure testing are clear: local properties are directly measured, specimens are less costly and more easily tested with better controlled test and environments.

Further efforts to extend the analytical techniques developed in the present study are recommended to include other typical substructure configurations and end conditions. Associated experimental techniques should also be generalized. The validity of the approach should be demonstrated with a comparision test on a complex structural specimen: measuring substructural properties and predict responses of the assembled structure on the one hand, and applying the excitations on the structure and measure the results on the other.

REFERENCES

1. Ramirez, G. A., "Investigation of Linear Hysteresis Damping for Vibration of Dyanmic Systems, "LMSC/HREC A784659, Lockheed Missiles & Space Company, Huntsville, Ala., September 1967.

2. Harris, C. M., and C. E. Crede (eds.), Shock and Vibration Handbook, "Vol 4, Nonlinear Vibration," by H. N. Abramson, McGraw-Hill, New York, 1961.

3. Chang, C. S., and R. E. Bieber, "Synthesis of Structural Damping," Final Report, Contract NAS8-20387, LMSC/HREC A783875, Lockheed Missiles & Space Company, Huntsville, Ala., March 1967.

4. Mixon, Catherine, and Arman, "Investigation of the Lateral Vibration Characteristics of a 1/5-Scale Model of Saturn SA-1," NASA TN D1593 (1963).

5. Timoshenko, S. P., Strength of Materials, 2nd edition, Part 2, D. Van Nostrand Co., Princeton, N. J.

6. Whiteman, I. R., "A Mathematical Model Depicting the Stress-Strain Diagram and the Hysteresis Loop," J. Appl. Mech., Vol 26 (1959) pp 95-100.

Appendix A

ESTIMATED MATERIAL DAMPING AND AIR DAMPING

Appendix A

Damping due to dissipation within the material and damping due to air drag are estimated for the 1/5-scale booster model of Saturn SA-I. Results for test Configuration I indicate that damping due to these factors are only a negligible portion of the total measured damping.

From Lazan* it is determined that for the test specimen material (2024-T4), the damping law is

$$D = J\sigma^n$$

where D is the energy dissipated per unit volume per cycle of steady-state oscillation at a uniaxial stress amplitude, σ, and J and n are damping properties, and

$$n = 2.0$$

and

$$J = 3.82 \times 10^{-11}.$$

The maximum potential energy density during a cycle is

$$P = \frac{\sigma^2}{2E}$$

so that

$$D = 2JE\,P.$$

* Lazan, B. J., Damping of Materials and Members in Structural Mechanics, Pergamon Press, Long Island City, N.Y., 1968.

The total energy dissipated in a cycle is

$$\int_V D dv = 2JE \int P dv = 2JE K$$

where K is the peak total kinetic energy of the model. If the only damping in the test specimen is due to material dissipations, the work done per cycle by an excitation force, F, at resonant frequency is

$$\pi FX = 2JE K.$$

Since $$K = \frac{1}{2} M \omega_1^2 z^2$$

$$M = 0.1864 \text{ lb-sec}^2/\text{in.}$$
$$E = 10.7 \times 10^6 \text{ lb/in}^2$$

the material damping force

$$F = JEM\omega_1^2 z/\pi$$

$$= \frac{3.82 \times 10^{-11} \times 10.7 \times 10^7 \times .01864}{\pi} \omega_1^2 Z$$

For $$\omega_1^2 z = 981.6 \text{ in/sec}^2,$$

$$F = 0.0226 \text{ lb}$$

The total measured damping force for the above condition (Columns 2 and 3, Table 2a) is 4.528 lb, some 200 times greater than the material damping force.

The aerodynamic drag at station x of the specimen in Configuration I is

$$f(x,t) = \frac{1}{2} \rho_a C_D(x)\, A(x)\, \dot{w}(x,t) \left|\dot{w}(x,t)\right|$$

where ρ_a = mass density of air

$C_D(x)$ = drag coefficient

$A(x)$ = projected area per unit length of model

$\dot{w}(x, t)$ = velocity of model at x

In the stady-state,

$$w(x, t) = w(\ell)\, \Phi(x) \sin \omega t$$

where $w(\ell)$ = tip deflection

$\Phi(x)$ = mode shape

The drag is, then,

$$f(x, t) = \frac{1}{2} \rho_a \omega_1^2 w^2(\ell)\, C_D(x)\, A(x)\, \Phi^2(x) \cos \omega t \left|(\cos \omega t)\right|$$

The fundamental component of the above force is in quadrature with the displacement, with an amplitude of

$$p(x) = \int_0^{2\pi/\omega} f(x, t) \cos \omega t \, dt = \frac{4}{3\pi} \rho_a \omega_1^2 w^2(\ell)\, C_D(x) A(x) \Phi^2(x)$$

The generalized damping force is

$$q = \int_0^{\ell} p(x)\, \Phi(x)\, dx$$

$$= \frac{4}{3\pi} \rho_a \omega_1^2 w^2(\ell) \int_0^{\ell} C_D(x)\, \Phi^3(x)\, A(x)\, dx.$$

For the same test point used to estimate material damping,

$$\omega_1^2 w^2(\ell) = 132.8 \text{ (in/sec)}^2$$

and $\rho_a = 1.12 \times 10^{-7}$ lb-sec^2/in^4

C_D = 2.0 fcr the spider-beam

C_D = 1.2 for the center LOX tank

and using the calculated made shape $\Phi(x)$, it is found that the aerodynamic damping force is

$$q = 0.0121 \text{ lb}$$

which is also negligibly small compared with the measured total damping force.